Reactive scattering of H2 from Cu(100): Comparison of dynamics calculations based on the specific reaction parameter approach to density functional theory with experiment

L. Sementa, M. Wijzenbroek, B. J. van Kolck, M. F. Somers, A. Al-Halabi et al.

Citation: J. Chem. Phys. **138**, 044708 (2013); doi: 10.1063/1.4776224
View online: http://dx.doi.org/10.1063/1.4776224
View Table of Contents: http://jcp.aip.org/resource/1/JCPSA6/v138/i4
Published by the American Institute of Physics.

Reactive scattering of H_2 from Cu(100): Comparison of dynamics calculations based on the specific reaction parameter approach to density functional theory with experiment

L. Sementa,[1,2,a)] M. Wijzenbroek,[1] B. J. van Kolck,[1] M. F. Somers,[1] A. Al-Halabi,[1] H. F. Busnengo,[3] R. A. Olsen,[1,4] G. J. Kroes,[1] M. Rutkowski,[5] C. Thewes,[5] N. F. Kleimeier,[5] and H. Zacharias[5]

[1]*Leiden Institute of Chemistry, Gorlaeus Laboratories, Leiden University, P.O. Box 9502, 2300 RA, Leiden, The Netherlands*
[2]*CNR-IPCF, Istituto per i Processi Chimico-Fisici of the Consiglio Nazionale delle Ricerche, Molecular Modeling Laboratory, I-56124 Pisa, Italy*
[3]*Instituto de Física Rosario (CONICET-Universidad Nacional de Rosario), A. Pellegrini 250, (2000) Rosario, Argentina*
[4]*SINTEF Materials and Chemistry, P.O. Box 124 Blindern, N-0314 Oslo, Norway*
[5]*Physikalisches Institut, Westfälische Wilhelms-Universität, D-48149 Münster, Germany*

(Received 13 July 2012; accepted 2 January 2013; published online 25 January 2013)

We present new experimental and theoretical results for reactive scattering of dihydrogen from Cu(100). In the new experiments, the associative desorption of H_2 is studied in a velocity resolved and final rovibrational state selected manner, using time-of-flight techniques in combination with resonance-enhanced multi-photon ionization laser detection. Average desorption energies and rotational quadrupole alignment parameters were obtained in this way for a number of ($v = 0, 1$) rotational states, v being the vibrational quantum number. Results of quantum dynamics calculations based on a potential energy surface computed with a specific reaction parameter (SRP) density functional, which was derived earlier for dihydrogen interacting with Cu(111), are compared with the results of the new experiments and with the results of previous molecular beam experiments on sticking of H_2 and on rovibrationally elastic and inelastic scattering of H_2 and D_2 from Cu(100). The calculations use the Born-Oppenheimer and static surface approximations. With the functional derived semi-empirically for dihydrogen + Cu(111), a chemically accurate description is obtained of the molecular beam experiments on sticking of H_2 on Cu(100), and a highly accurate description is obtained of rovibrationally elastic and inelastic scattering of D_2 from Cu(100) and of the orientational dependence of the reaction of ($v = 1$, $j = 2 - 4$) H_2 on Cu(100). This suggests that a SRP density functional derived for H_2 interacting with a specific low index face of a metal will yield accurate results for H_2 reactively scattering from another low index face of the same metal, and that it may also yield accurate results for H_2 interacting with a defected (e.g., stepped) surface of that same metal, in a system of catalytic interest. However, the description that was obtained of the average desorption energies, of rovibrationally elastic and inelastic scattering of H_2 from Cu(100), and of the orientational dependence of reaction of ($v = 0$, $j = 3 - 5, 8$) H_2 on Cu(100) compares less well with the available experiments. More research is needed to establish whether more accurate SRP-density functional theory dynamics results can be obtained for these observables if surface atom motion is added to the dynamical model. The experimentally and theoretically found dependence of the rotational quadrupole alignment parameter on the rotational quantum number provides evidence for rotational enhancement of reaction at low translational energies. © *2013 American Institute of Physics*. [http://dx.doi.org/10.1063/1.4776224]

I. INTRODUCTION

The dissociative adsorption of molecules on surfaces is relevant to a number of industrial applications. It is a fundamental step in corrosion and hydrogen storage in metals. It can also be a key step in heterogeneous catalysis, especially if the dissociation of one of the reactants is activated, making it the rate-limiting step of the overall reaction (an example being N_2 dissociation in NH_3 synthesis).[1] Being able to model such key reaction steps accurately is also relevant for practical purposes, as roughly 90% of the chemical manufacturing processes used throughout the world employ catalysts in one form or another.[2]

Theorists who aim to describe such key reaction steps accurately in the framework of modeling heterogeneous catalysis or to extract insights in the dynamics of the reaction step face at least three challenges.[3,4] First, the extraction of accurate reactive scattering results may require modeling the effect of electron-hole (e-h) pair excitation, as suggested for associative desorption of N_2 from Ru(0001)[5] and as shown

a)Author to whom correspondence should be addressed. Electronic mail: luca.sementa@ipcf.cnr.it.

for non-reactive scattering of NO from metal surfaces.[6,7] Second, the extraction of accurate results may also require modeling the effect of phonons, especially for molecules that are "heavy" compared to H_2, like N_2[8] and CH_4.[9] Third, the electronic structure methods which may now be used to map out potential energy surfaces (PESs) for molecule-metal surface systems or in *ab initio* molecular dynamics (AIMD) calculations on these systems (density functional theory (DFT) at the generalised gradient approximation (GGA) or meta-GGA level) are not yet able to provide reaction barrier heights with chemical accuracy (errors < 1 kcal/mol), as evidenced by research on databases on gas phase reactions.[10–12] For a thorough understanding of and for quantitatively accurate modeling of catalysis, it is this accuracy ("chemical accuracy") that one would want to achieve in electronic structure modeling.

H_2-metal surface systems represent a natural choice of system if the aim of a study is to test the accuracy of an electronic structure approach for computing the interaction of a molecule with a metal surface. The reason for this is that, for these systems, many observables can be computed with high accuracy with a dynamical model (the Born-Oppenheimer static surface (BOSS) model) in which e-h pair excitation and phonons are neglected. For instance, research that used friction coefficients to model e-h pair excitation showed very small electronically non-adiabatic energy losses in reactive scattering of H_2 from Cu(111)[13] and Cu(110),[14] so that the sticking probability of H_2 on Cu(110) is hardly affected by e-h pair excitation.[14] Other evidence for the high accuracy that can be achieved for reactive scattering of H_2 from metal surfaces comes from calculations on H_2 + Pt(111), which showed that accurate results for both sticking and diffractive scattering could be obtained using a single PES and neglecting e-h pair excitation.[15] This was used to argue that the reactive scattering of H_2 from Pt(111) should not be affected to a large extent by energy dissipation to e-h pairs, for reasons that are generic to H_2-metal surface systems (for details, see Ref. 15). In a notable exception, reduced dimensionality dynamics calculations on H_2 + Cu(111), which modeled motion in two H_2 degrees of freedom and one surface mode and used friction coefficients to model e-h pair excitation, suggest that energy dissipation to e-h pairs may be required to obtain the correct energy and isotope dependence of vibrational de-excitation of H_2[16] and D_2[17] scattering from Cu(100).

For H_2-metal surface systems, a number of observables can likewise be computed with high accuracy while neglecting phonons, using a static surface model. For instance, static surface quasi-classical trajectory (QCT) calculations modeling sticking of D_2 to Cu(111) at low surface temperature ($T_s = 120$ K) using a PES obtained with the specific reaction parameter (SRP) approach[18] to DFT are in excellent agreement with AIMD results obtained with SRP-DFT,[19] which modeled phonon motion. Another observable that can be computed reasonably accurately with the static surface model is the so-called effective barrier height $E_0(v, j)$, which corresponds to the translational energy for which the reaction probability of H_2 in its initial vibrational state v and rotational state j first becomes equal to half the maximum experimental value.[20] Experiments[20,21] suggest that this observable hardly depends on T_s, while the dependence of the reaction probability curve on incidence energy can be modeled by making the width of the reaction probability curve dependent on T_s. These findings are in agreement with calculations in which simple methods are used to model the energy transfer from the molecule to a single surface atom.[22]

Calculations using the static surface approximation on reactive H_2-metal surface scattering should nevertheless exercise caution in the interpretation of the results. Experiments[21] suggest that below the classical reaction threshold the effect of T_s on reaction cannot be described by a simple broadening effect, and similar threshold effects on reaction as well as inelastic scattering have been confirmed in quantum dynamics calculations on H_2 + Cu(111).[23] In comparing static surface theoretical results to measured mean kinetic desorption energies, the broadening effect of T_s on the width of the reaction probability curve should be taken into account[24] (see also below). AIMD calculations show that raising T_s affects the dependence of reaction on molecular orientation, leading to reduced rotational quadrupole alignment parameters of D_2 molecules desorbing from Cu(111) at high T_s.[19] Finally, experiments on rotational excitation accompanied by vibrational de-excitation of H_2 scattering from Cu(100) and Cu(110) shows that these processes can be accompanied by considerable energy loss to the surface,[16] while calculations[25] using the BOSS model and SRP-DFT to model vibrational excitation of H_2 scattering from Cu(111) clearly show that modeling phonons should be required to reproduce experiments[26] on vibrational excitation of H_2 on Cu(111).

Recently a new implementation[18] of a semi-empirical SRP-DFT approach[27] was introduced, which allowed the modeling of reactive scattering of H_2 from Cu(111) with chemical accuracy.[18] In the new implementation[18] SRP-DFT was adapted to the calculation of molecule surface interaction energies by taking the SRP density functional as a weighted average of two GGA functionals popular in surface science, i.e., the PW91[28] and the RPBE[29] functionals. In the procedure adopted, the SRP functional was fit by requiring that the QCT calculations using the PES computed with this functional reproduce experiments that are sensitive to the reaction barrier height for the specific system considered, i.e., molecular beam experiments on D_2 + Cu(111) that had provided reaction probabilities for collision energies up to 0.8 eV at $T_s = 120$ K. The PW91[28] and RPBE[29] functionals were selected because these functionals systematically overestimate and underestimate the reactivity of H_2 on Cu(111).[18] Another idea underlying the SRP-DFT approach is that with the functional thus obtained it should be possible to describe other experiments, including more detailed scattering experiments, with high accuracy. In accordance with this idea, the SRP PES subsequently allowed sticking experiments on H_2 + Cu(111), associative desorption experiments investigating the dependence of the reaction probability on the initial rovibrational state of H_2, and experiments on rotationally inelastic scattering of H_2 ($v = 1$, $j = 0$) from Cu(111) to be reproduced with chemical accuracy. As already noted above, with the BOSS model and the SRP-DFT PES it was not possible to reproduce some other observables,[19,25] but thanks in part to the established accuracy of the SRP-DFT PES these failures could

be attributed in large part to one of the shortcomings of the BOSS model, i.e., the static surface approximation.

As already noted, calculations on the dissociation of molecules on metal surfaces may be relevant to the modeling of heterogeneous catalysis. The semi-empirical SRP-DFT approach described above would obviously have added value if SRP functionals, which are obtained through comparison with surface science experiments involving the molecule of interest interacting with a low index metal surface, can be shown to also work for that molecule interacting with defected (for instance, stepped) surfaces of that metal, as these surfaces are often of greater interest to catalysis.[30–32] As a first step in this direction, the central question raised in the present study is whether the SRP-GGA functional derived semi-empirically for H_2 + Cu(111) is "transferable" to H_2 interacting with another low index Cu surface, the (100) surface. A positive answer can obviously be taken as an encouragement to study transferability of SRP-functionals developed for low index surfaces to defected surfaces. The more specific question we ask in this study is whether the SRP functional developed for H_2 + Cu(111) allows one to accurately reproduce experimental results for H_2 + Cu(100). For this purpose, we compare results of quantum dynamics calculations on reactive scattering of H_2 from Cu(100), which are based on a PES obtained with the functional optimized for H_2 + Cu(111), to several experiments, including new associative desorption experiments that are presented here on the orientational dependence of the reaction, and on the effect of the initial rovibrational state of H_2 on the reaction. In making the comparison, we use the BOSS model described above, which of course implies that for each observable addressed we have to carefully consider the possible impact of the dynamical approximations made on our theoretical results, and how this may affect the comparison to experiment.

The dissociative chemisorption of H_2 and D_2 on Cu(100) has been widely studied experimentally. The role of the translational and vibrational energy in the dissociation process was studied with associative desorption experiments using D_2[33] and with molecular beam experiments using normal and off-normally incident H_2.[34] The molecular beam experiments established that the dissociation of H_2 on Cu(100) is activated and is, to at least a good approximation, a function of the normal component of the incident energy only (normal energy scaling). The measured sticking probabilities were later analyzed as sums of contributions of molecules in different vibrational states having different threshold behaviors (multiple state model).[35] The analysis showed that dissociation of H_2 on Cu(100) is enhanced if the incident molecule is initially vibrationally excited, i.e., about 60% of the energy of the vibrational quantum is used to overcome the barrier for dissociative adsorption. This is also supported by vibrationally state-resolved measurements of the angular distribution in desorption of H_2 and D_2 from Cu(100).[36] Vibrationally excited molecules showed a significantly broader angular distribution than the ground state molecules, as expressed in the exponent of the $\cos^n\theta$ distributions. This trend could be described in a 2D calculation for H_2 + Cu(111).[37] The sticking probability of high temperature seeded beams should be dominated by vibrationally excited molecules at low incident energies.

Rovibrationally elastic and inelastic scattering probabilities of H_2 prepared in the $(v = 1, j = 1)$ state were measured for scattering to several final (v, j) states for incident energies in the range 35–200 meV.[16] The sum of all measured elastic and inelastic scattering probabilities was substantially less than one, and the "loss" (the probability of scattering to channels not accounted for) increased from 35% at about 75 meV to 50% at 200 meV. The loss was argued to be due to either a large probability for $(v = 1 \rightarrow 0)$ vibrational relaxation into two rotational states, which could not be observed in the experiments because of the high thermal population in those states $(v = 1, j = 1, 3)$, or to dissociative chemisorption. A dissociation channel of magnitude equal to the loss was argued to be inconsistent with probabilities determined from previous energy- and state-resolved desorption experiments. This is borne out by recent measurements on the sticking of $(v = 1, j = 1)$ H_2 on Cu(100) using laser-induced thermal desorption, in which upper bounds to the state-resolved dissociation probabilities could be determined which are inconsistent with the loss being predominantly due to reaction.[38]

State-resolved experiments were also published for the scattering of D_2 $(v = 1, j = 2)$ from Cu(100).[17] The primary motivation for this work was to compare the scattering of vibrationally excited D_2 to that of H_2 from the same surface, as the different energy content of the molecules in their respective initial states allow one to explore different regions of an otherwise identical PES. The experiments showed that the survival probability is greater for $(v = 1)$ D_2 than for $(v = 1)$ H_2 on Cu(100) at similar incident energies. At variance with H_2, for D_2 the sum of all elastic and inelastic scattering probabilities was very close to one, the transition probabilities to $(v = 1, j = 0)$ and $(v = 1, j = 4)$ accounting for the missing fraction of molecules in the survival probability measurement for most of the incident energies measured.

The H_2 + Cu(100) system has also been the subject of many theoretical studies. The earliest six-dimensional (6D) quantum dynamics calculations to be published on activated dissociative chemisorption were performed on this system.[39] Subsequent 6D quasi-classical[40] and quantum dynamics calculations[41,42] explored the effect of the initial rotation of H_2 on the reaction on Cu(100), and on the vibrational excitation[43] of H_2 on Cu(100). Next, 6D quantum dynamics calculations were used to explore rovibrationally (in)elastic scattering of $(v = 1, j = 1)$ from Cu(100) in a joint experimental-theoretical paper,[44] and in subsequent theoretical work based on a more accurately fitted potential energy surface.[45] The system was also used to uncover experimental signatures of site reactivity in work bearing a close relationship to the present work, as the suggested experimental signature involves the relationship between measured rotational quadrupole alignment parameters of H_2 $(v = 0, j)$ and $(v = 1, j)$ just above the reaction threshold.[46,47] H_2 + Cu(100) was also used as a benchmark to demonstrate a new, symmetry adapted pseudospectral method.[48] Finally, more recently the system has been used to explore the applicability of a mean field quantum dynamics method to investigate

the effect of phonons on reactive and non-reactive scattering of H_2 from copper surfaces.[49,50]

Here, we present new results of energy resolved rovibrational state selective associative desorption experiments on H_2 desorbing from Cu(100) at a surface temperature (T_s) of 1030 K. An interpretation based on detailed balance allows information to be extracted on the effect of the initial rovibrational state and reagent angular momentum alignment on dissociative chemisorption: Using an improved detection scheme the quadrupole alignment factor $A_0^{(2)}$ is also obtained as a function of H_2 kinetic energy. These experiments, and the results of the earlier experiments discussed above are compared to results of quantum dynamics calculations using the BOSS model, and employing a PES computed with the SRP functional developed for hydrogen reacting with Cu(111).

The comparison of the theory to the earlier and the new experiments shows that the SRP functional developed for H_2 + Cu(111) yields a chemically accurate description of the sticking probability curve measured in molecular beam experiments for H_2 + Cu(100). Our calculations also give a very accurate description of the rotationally inelastic scattering experiments on D_2 + Cu(100). The theoretical description obtained of rotationally elastic and inelastic scattering of H_2 from Cu(100) was not as accurate as that obtained for D_2, but the description obtained for H_2 is improved when compared to earlier theoretical work and remaining discrepancies can be due to shortcomings of the BOSS model. The calculations tend to underestimate the average translational energy of H_2 desorbing into the ($v = 0$), and ($v = 1$) rotational states studied in the new experiments. The calculations give a reasonably accurate description of the rotational quadrupole alignment parameter of (v, j) H_2 desorbing from Cu(100), but the experimental results are not yet reproduced quantitatively.

The outline of the paper is as follows. Section II A describes the apparatus and how desorption experiments were carried out. In Sec. II B, we outline the theoretical model and we briefly describe the aspects of the PES. In Secs. III A and III B, the outcomes of the new experiments and the calculations are described separately. In Sec. IV, the theoretical results are compared with previously measured sticking probabilities and the newly measured average desorption energies (ADEs) (Sec. IV A), the newly measured rotational alignment parameters (Sec. IV B), and the previously measured rovibrationally (in)elastic scattering probabilities for H_2 and D_2 (Sec. IV C). The conclusions are summarized in Sec. V.

II. METHOD

A. Desorption experiments

The experiments are performed in an ultra-high vacuum chamber pumped by turbomolecular and titanium getter pumps to a base pressure of less than 2×10^{-10} mbar. Order and cleanliness of the surface are determined by low-energy electron diffraction and Auger spectroscopy. When necessary adsorbates are removed by soft Ar^+ ion sputtering, the surface is allowed to anneal before the desorption experiments are carried out.

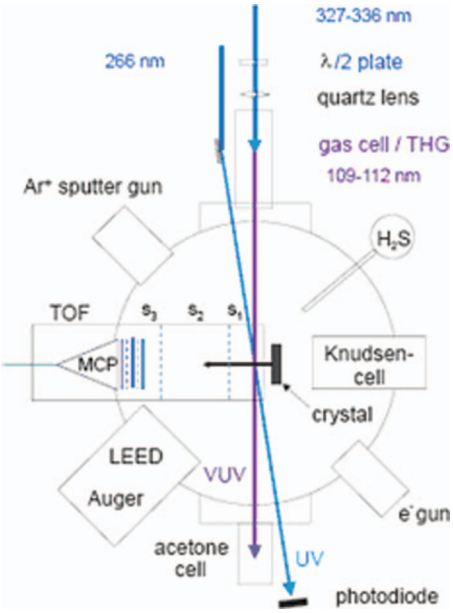

FIG. 1. Schematic diagram of the experimental setup. The exciting VUV and the ionizing UV laser cross in a plane parallel to the copper surface at a distance of 15 mm. See the text for the definition of s_1, s_2, and s_3.

Hydrogen atoms are supplied to the surface by atomic permeation through the bulk of the 1 mm thick single crystal. The sample is radiatively heated to a temperature of 1030 K and subsequently kept at this temperature. During hydrogen desorption the average chamber pressure increased to about 10^{-8} mbar although an additional cryopump (pumping speed 2.500 l/s) was operational. Knowing thus the permeation rate of hydrogen through the copper crystal,[51] kinetic desorption parameters and the effective pumping speed one can estimate that the average hydrogen coverage on the surface is less than about 1% of a monolayer. After desorption the hydrogen molecules follow a flight path of 15 mm through a 5 mm diameter aperture into a field-free time-of-flight (TOF) detector (Fig. 1). This time-of-flight detector allows not only to measure the rotationally resolved kinetic energy distribution, but also to discriminate against the gas phase background, because the desorbing molecules are generally significantly faster than those from the gas phase.

Rotational state selective detection of desorbing molecules is performed by (1 + 1′) REMPI. Hydrogen molecules are electronically excited in the B $^1\Sigma_u^+(v'', j'')$ ← X $^1\Sigma_g^+(v, j)$ Lyman system with vacuum ultraviolet radiation (VUV) tunable in the $\lambda = 109.8$–111.6 nm spectral range (note that we use the notation v and j for the vibrational and rotational quantum numbers of H_2 in its electronic ground state, and v'' and j'' for the quantum numbers in the excited electronic state. Further as common in theoretical work, we use (v', j') to denote the final rovibrational state the H_2 molecule is scattered to in its electronic ground state).

The VUV radiation is generated by frequency tripling the second harmonic of tunable dye laser radiation in krypton and xenon gas. Pulse energies of about 1.5 nJ in the VUV are employed. Various rovibrational transitions in the Lyman (0-0) to (3-0) and (3-1) to (5-1) bands are used to determine rotational populations in the ground and vibrationally excited

states of molecular hydrogen. The excitation beam is focused to a beam diameter of about 0.8 mm in the ionization volume. Using the band oscillator strengths of Allison and Dalgarno[52] and a pulse duration of about 5 ns this yields excitation rates of about 8×10^4 s^{-1}, which is small compared to the B state spontaneous emission rate of 1.2×10^9 s^{-1}.[53] A second UV photon at $\lambda = 266$ nm, with a pulse energy of 3.5 mJ, derived by frequency quadrupling radiation of the fundamental Nd:YAG laser, ionizes the electronically excited molecules. The UV and VUV beams are intersecting in a plane parallel to the sample surface at a distance of 15 mm from the sample. The ionizing radiation is always linearly polarised parallel to the surface normal, while the linear polarisation of the exciting VUV radiation could be varied from parallel to perpendicular to the surface normal. This variation of the VUV polarisation enables the determination of the rotational alignment of the desorbing molecules.

The kinetic energy distribution of the desorbing hydrogen molecules is determined via a field-free time-of-flight of the resonantly ionized and thus rovibrational state selectively produced photoions.[54] In this specific realisation, the H_2^+ photoions are produced in a three-stage time-of-flight tube to enhance the detection sensitivity, and are detected by microchannel plates. In the first stage, they are slightly ($a_1 = 1.25$ V/cm) accelerated over a distance of $s_1 = 22$ mm towards a field-free drift tube of $s_2 = 65$ mm length. At the end of this drift tube, a second acceleration ($a_3 = 110$ V/cm) over $s_3 = 7$ mm directs the ions into the microchannel plate detector. The total flight time of the ions is then the sum of the flight times through these three stages, and correspondingly

$$\frac{dt_{ges}}{d\upsilon} = \left|\frac{dt_1}{d\upsilon}\right| + \left|\frac{dt_2}{d\upsilon}\right| + \left|\frac{dt_3}{d\upsilon}\right| \tag{1}$$

with

$$\frac{dt_1}{d\upsilon} = -\frac{1}{a_1} + \frac{\upsilon}{a_1\sqrt{\upsilon^2 + 2s_1a_1}}, \tag{2a}$$

$$\frac{dt_2}{d\upsilon} = \frac{s_2\upsilon}{\sqrt{(\upsilon^2 + 2s_1a_1)^3}}, \tag{2b}$$

$$\frac{dt_3}{d\upsilon} = \frac{\upsilon}{a_3\sqrt{\upsilon^2 + 2s_1a_1 + 2s_3a_3}} - \frac{\upsilon}{a_3\sqrt{\upsilon^2 + 2s_1a_1}}, \tag{2c}$$

where s_i are the lengths of the stages i and a_i are the accelerations in these stages, as previously defined. The accelerations a_i are calculated from

$$a_i = \frac{qU_i}{ms_i}. \tag{3}$$

Here, q denotes the charge state of the ions, U_i the accelerations voltage, and m the mass of the ions.

Figure 2 shows a typical time-of-flight signal obtained from a gas phase molecular hydrogen sample using the time-of-flight detector described above. The full line shows the measured distribution, the open circles a fit for a volume Maxwell-Boltzmann distribution. When fitting the measured arrival time signal, hydrogen ion sources distributed over a region of 0.8 mm diameter have been taken into account in order to correct for the finite width of the detection laser beams. This finite distribution of the starting points of the ions has a visual noticeable effect only for extremely slow molecules with kinetic energies well below 10 meV, or in the time-of-flight spectra between about 7.5 and 7.7 μs. Although these energies are not relevant in the present investigation all fits contained the integration over the laser beam diameter. A very good agreement of the measured and the expected Maxwell-Boltzmann distributions is obtained, giving confidence in the measuring and fitting procedure. From such a fit the actual important acceleration in the first section can be derived, accounting also for spuriously changing contact potentials. Therefore, after each measurement of desorbing hydrogen molecules such a calibration run on gas phase hydrogen molecules has been performed.

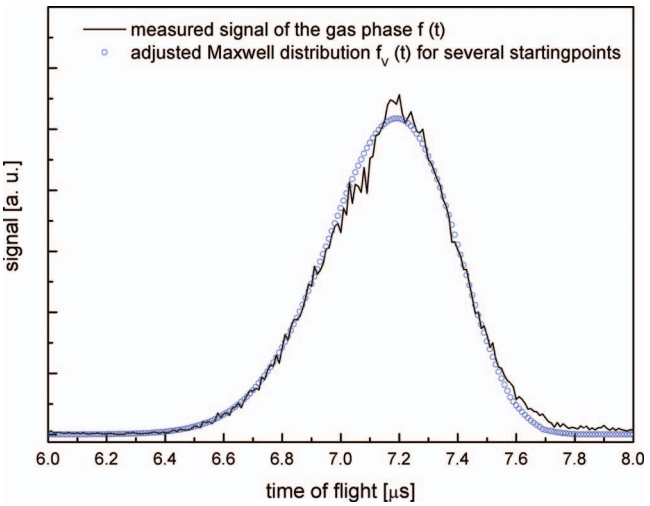

FIG. 2. Time-of-flight signal obtained from a gas phase molecular hydrogen sample using the time-of-flight detector described in the text.

Information about the rotational angular momentum alignment is obtained by measuring the arrival times with the VUV probe laser beam being polarised parallel ($I_\parallel$) and perpendicular ($I_\perp$) to the surface normal. The ionization step has been saturated for both polarisations. From this measurement an anisotropy P can be defined by $P = (I_\parallel - I_\perp)/(I_\parallel + I_\perp)$. With this, the rotational angular momentum quadrupole alignment $A_0^{(2)}$ can be derived for the P and R rotational branches by the following equations:[55]

$$A_0^{(2)} = \frac{-4P(2j-1)}{(j+1)(3-P)} \quad \text{(P branch)} \tag{4a}$$

and

$$A_0^{(2)} = \frac{-4P(2j+3)}{j(3-P)} \quad \text{(R branch)}. \tag{4b}$$

Since the time-of-flight data yield signal intensities as a function of time delay after ionization, after transformation to the velocity, or translational energy domain, the alignment can also be obtained as a function of translational energy.

B. Computational method

Our dynamical calculations treat the motion of H_2 (D_2) in all six degrees of freedom at quantum level. We refer the reader to the supplementary material[56] and earlier work (Ref. 18) for a detailed discussion of the model and how

quantities that are comparable to observables measured in molecular beam experiments and associative desorption can be obtained from computed initial state-resolved reaction probabilities $R_{v\,j\,m_j}(E)$ and degeneracy averaged reaction probabilities $R_{v\,j}(E)$.

To obtain the potential energy surface, we use the specific reaction parameter approach to DFT,[27] in an implementation[18] that is adapted to the calculation of molecule-surface interaction energies. This approach, originally applied to gas phase reactions, already allowed the accurate modeling of reactive scattering of H_2 from Cu(111). In the SRP-DFT approach used, the exchange-correlation part of the SRP functional is a weighted average of the exchange-correlation parts of the PW91 and RPBE functionals

$$E_{xc}[\rho] = x E_{xc}^{RPBE}[\rho] + (1-x)E_{xc}^{PW91}[\rho]. \qquad (5)$$

In Eq. (5), x was set to 0.43 to obtain the semi-empirically derived SRP-GGA functional used to describe the Cu(111) + H_2 system. The density ρ was obtained self-consistently from the PW91 functional, whereas the RPBE energy was obtained non-self-consistently from the PW91 density to avoid the extra computational expense associated with self-consistent RPBE calculations. The SRP energies constituting the PES therefore also are non-self-consistent results, being obtained from PW91 densities. For H_2 + Cu(111), test calculations in which RPBE energies were computed self-consistently showed that the approximation used does not significantly affect the accuracy of the molecule-surface interaction energies, leading to absolute errors less than 0.12 kcal/mol.[18] Because the SRP functional interpolates between the PW91 energies and RPBE energies, differences between non-self-consistent and self-consistent SRP energies are expected to be even smaller.[18] It is believed that these arguments also hold for the current H_2 + Cu(100) system. The assumption tested here is that the expression of the SRP functional and the x value in it previously obtained for H_2 + Cu(111) is also good for describing H_2 interacting with another low index face of Cu, i.e., Cu(100).

In Fig. 3, the most essential aspects of the H_2/Cu(100) SRP-DFT PES are shown. The lowest barrier (0.74 eV) found for the dissociation geometries investigated corresponds to dissociation above the bridge site with the H atoms moving towards the hollow sites and H_2 oriented parallel to the surface (see also Table I). The highest barrier found above a high-symmetry site corresponds to H_2, oriented parallel to the surface, dissociating above the top site with the H atoms moving towards the bridge sites (0.90 eV). The analysis of the PESs obtained with the PW91 and RPBE functionals shows that their shapes hardly depend on the functional used, although the barrier heights in these PESs differ from the SRP-PES values in absolute value by at least 130 meV for the top to bridge dissociation route and by at least 150 meV for the other geometries. Impact on the top site has been found to be relevant for vibrationally inelastic scattering and for dissociation of vibrationally excited and highly rotationally excited H_2 on Cu(100).[40,46,57] The 2D elbow for this dissociation route shows a large curvature of the reaction path and an especially late barrier (occurring at a large H–H distance r, see Fig. 3 and Table I). These two features are known to promote vibrationally inelastic scattering.[40,58,59] Likewise, the later the barrier at a site is, the more reaction at that specific site should be promoted by rotational pre-excitation to high j and/or by vibrational pre-excitation.[40,46]

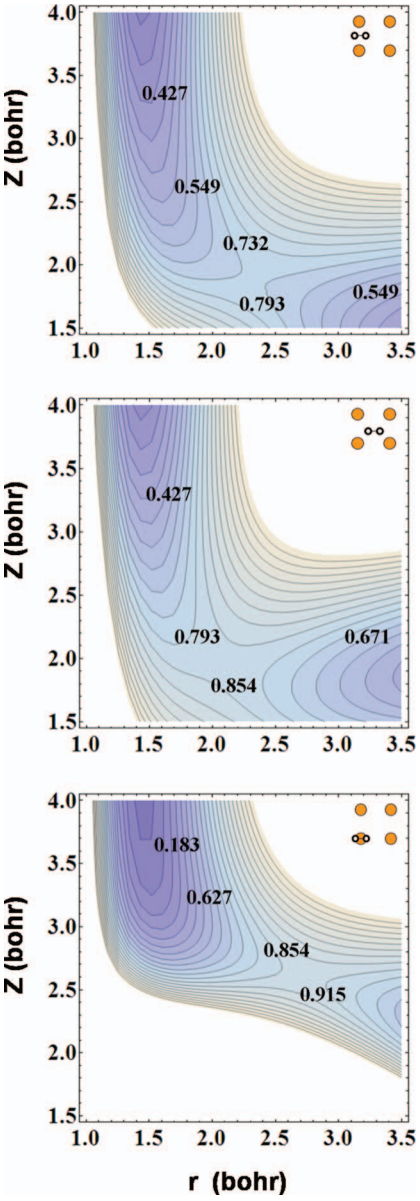

FIG. 3. H_2 + Cu(100) SRP-PES. Two-dimensional cuts are shown for three different reaction routes: (top panel) bridge-to-hollow dissociation, (middle panel) hollow-to-bridge dissociation, and (bottom panel) top-to-bridge dissociation. In each case, H_2 is oriented parallel to the surface. Contour lines (energies in eV) have a spacing of 61 meV. Each decimal point is located on the relative iso-line.

TABLE I. Barrier locations, heights (eV) and measures of ϑ and ϕ anisotropies are shown for the high-symmetry sites of the SRP-PES.

	Top	Hollow	Bridge
r (Bohr)	2.72	2.08	2.32
Z (Bohr)	2.60	1.96	1.90
Height (eV)	0.87	0.84	0.74
Anisotropy in ϕ (eV)	0.06	0.08	2.84
Anisotropy in ϑ (eV)	29.2	0.46	1.75

In Table I, barrier locations, heights, and measures of ϑ and ϕ anisotropies are shown for the high-symmetry sites. The polar (ϑ) anisotropy is defined by the range of potentials experienced by H_2 when located at the minimum barrier geometry and rotated out of the plane parallel to the surface, keeping all of the other degrees of freedom fixed. The azimuthal (ϕ) anisotropy is analogously defined by rotating the molecule parallel to the surface and keeping all the other degrees of freedom fixed at the minimum barrier geometry of a high-symmetry site. The top-site barrier is the "latest" and shows the largest polar anisotropy (29.2 eV), whereas the largest azimuthal anisotropy is found for the bridge site (2.84 eV). The hollow and top sites both show a weak azimuthal anisotropy at the corresponding barrier geometries, 0.06 and 0.08 eV, respectively. The site with the lowest polar anisotropy is the hollow site, which displays the earliest barrier of all the high-symmetry sites considered. Experience with earlier quantum dynamics calculations on H_2 + Cu(100) then suggests that at low collision energies molecules in the vibrational ground state $v = 0$ with low angular momentum quantum number j will react preferentially at the lowest barrier bridge site.[46] In contrast, vibrationally excited molecules and molecules with high j are likely to react preferentially at the top site, where vibrational and rotational energy may more easily be converted to energy in motion along the reaction path.[46]

III. RESULTS

A. Experimental results

Figure 4 shows a typical arrival time spectrum for ground state hydrogen molecules desorbing at $T_s = 1030$ K from Cu(100) in $j = 4$ obtained via the (1-0) P(4) line in the Lyman system. Two distinct signal peaks can clearly be identified. The slower one, arriving at t ~ 7.2 μs evidently arises due to molecules from a gas phase background, see Fig. 2. The faster one, arriving around t ~ 5.7 μs is caused by directly desorbing hydrogen molecules. The signal peaks show a different

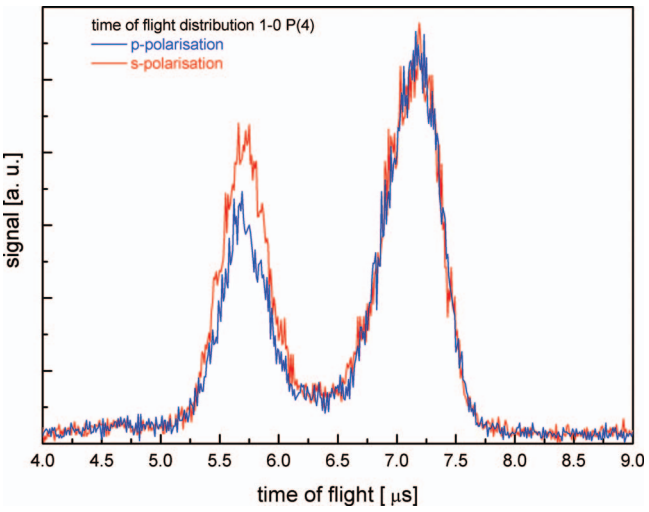

FIG. 4. Arrival time spectrum for ground state hydrogen molecules in $j = 4$ desorbing at $T_s = 1030$ K from Cu(100).

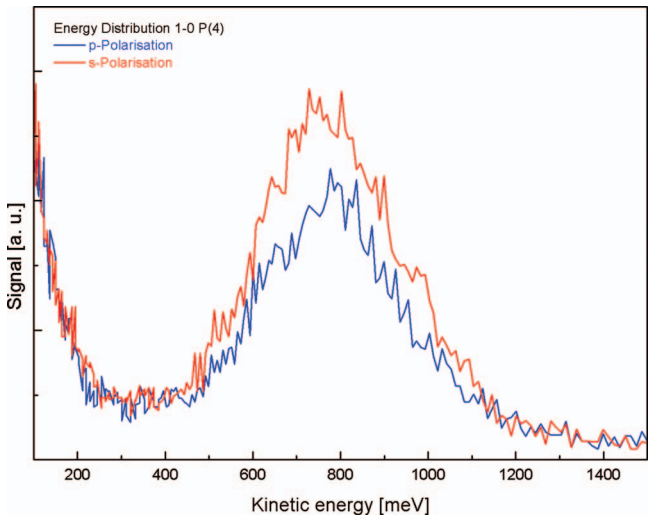

FIG. 5. Kinetic energy distribution of H_2 ($v = 0$, $j = 4$) for two polarisations of the probe laser radiation.

behavior with respect to the polarisation of the exciting VUV radiation. Whereas the slower gas phase signal is not sensitive to a change of the polarisation, the faster molecules show a pronounced difference. The signal is higher for a VUV polarisation perpendicular to (red line in Fig. 4) than for one parallel to (blue line in Fig. 4) the surface normal. This implies that a negative molecular anisotropy P is observed, which in turn yields a positive quadrupole alignment parameter, see Eq. (4a). A positive quadrupole alignment indicates a molecular ensemble with their $\boldsymbol{j}$-vectors predominantly parallel to the surface normal. The molecules thus execute a helicopter-type motion as they are desorbing from the copper surface.

Figure 5 shows the transformation of the arrival time spectrum into a plot versus the translational energy of the desorbing molecules. The kinetic energy distribution of directly desorbing H_2 molecules peaks around 750–800 meV kinetic energy.

Again the difference in intensity for the two polarisations can be noticed. Evaluating now the rotational alignment parameter according to Eq. (4b) yields the dependence of the alignment parameter on the kinetic energy, as shown in Fig. 6(a) for energies in the range up to 1200 meV. For the quadrupole alignment parameter averaged over the energy from 385 meV to 1400 meV a positive value of $A_0^{(2)} = (0.24 \pm 0.02)$ is obtained. Similar results, but with different values for $A_0^{(2)}$ are observed for ($v = 0$, $j = 1 - 5, 8$) and will be discussed below. Also for vibrationally excited molecules a positive alignment parameter is observed for all lines examined. Figure 6(b) shows the results for ($v = 1$, $j = 2 - 4$) up to 800 meV kinetic energy. Here, maximal alignment parameters of about $A_0^{(2)} = 0.30$–0.35 are obtained. In the vibrationally excited state, only $j = 2$–4 were examined. The data for ($v = 1$, $j = 1$) were obscured by an accidental resonant dissociation of the H_2 molecule into H(1s) + H(2s, 2p). The latter product is efficiently ionized and obscures in the arrival time spectrum the signal from directly desorbing H_2 ($v = 1$, $j = 1$).[54]

In addition to the energy dependent alignment results also the average translational desorption energies $\langle E_{kin} \rangle$ can be

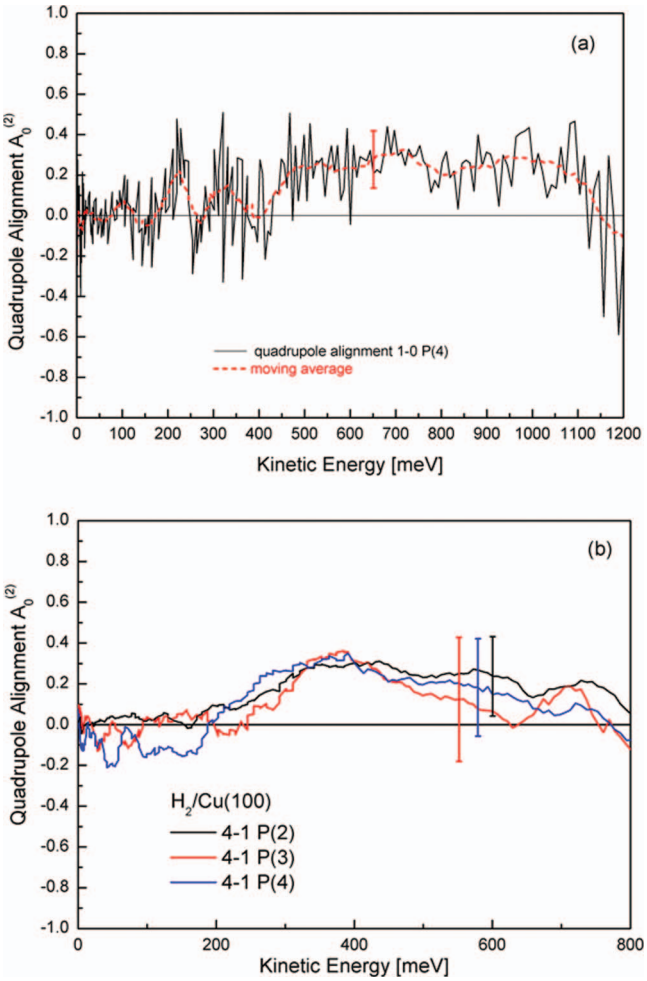

FIG. 6. (a) Dependence of the observed alignment parameter for ($v = 0$, $j = 4$) on the translational energy of desorbing H_2, as shown in Fig. 5 for energies up to 1200 meV. The black line shows the direct subtraction and thus raw data, while the dashed red line is a ten point moving average. (b) Same as before for ($v = 1$, $j = 2 - 4$), but showing only the average data. The error bars indicate the average error (68% confidence intervals) of the energy resolved alignment.

deduced from this data for each rotational state. As discussed in more detail below, for ground state H_2 molecules the highest $\langle E_{kin} \rangle = (880 \pm 20)$ meV is observed in $j = 1$, steadily decreasing to $\langle E_{kin} \rangle = (630 \pm 20)$ meV for $j = 8$. For vibrationally excited molecules, the average kinetic energies are significantly lower, being around $E_{kin} = (500 \pm 20)$ meV.

B. Computational results

1. Reaction

Degeneracy averaged reaction probabilities for four different initial rovibrational states are shown in Fig. 7. All curves have a sigmoidal shape with an onset that depends strongly on the rovibrational energy of the initial state. For initially non-rotating molecules in the vibrational ground state, the reaction probability is 0.1% at 0.59 eV. At this translational energy and considering zero-point effects the total energy of ($v = 0$, $j = 0$) H_2 is 0.85 eV, which is just 0.11 eV higher than the minimum energy barrier on the bridge site. Vi-

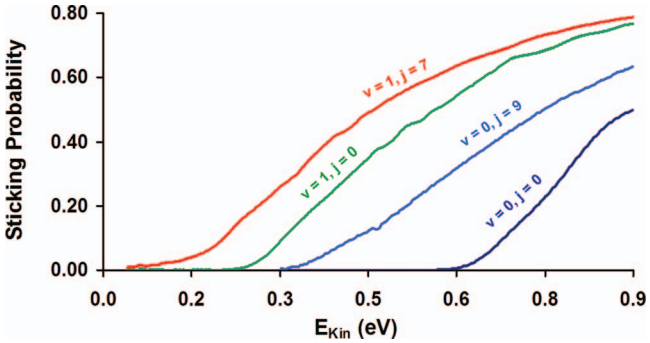

FIG. 7. Degeneracy averaged reaction probabilities $R_{v\,j}(E)$ computed for H_2, using the SRP density functional. Probabilities are given for various (v, j) initial states.

brationally excited molecules need less kinetic energy to dissociate, and the ($v = 1$, $j = 0$) reaction probability is 0.1% at 0.24 eV. Near the threshold the total energy of ($v = 1$, $j = 0$) H_2 is 1.01 eV, which is 0.13 eV higher than the minimum barrier height on the top to hollow dissociation route. At each collision energy in the considered range, also fast rotating ($v = 0$, $j = 9$) molecules dissociate more easily than molecules in the ground rovibrational state. Furthermore, it is interesting to note that even though ($v = 0$, $j = 9$) molecules have about 90 meV more internal energy than ($v = 1$, $j = 0$) molecules, the reaction probability curve of ($v = 1$, $j = 0$) H_2 is always above that of ($v = 0$, $j = 9$) H_2 so that the vibrational efficacy is higher than the rotational efficacy, as we found in experiments on H_2 + Cu(111).[66]

Figure 8(a) shows the theoretical sticking probabilities (calculated according to Eq. (S.7) of the supplementary material).[56] The fact that the theoretical sticking probabilities computed using two different methods to extract the parameters characterizing the velocity distributions (see Sec. S.3 of the supplementary material)[56] hardly differ suggests that the computed sticking probabilities are not very sensitive to potential errors arising from the characterization of the velocity distributions describing the molecular beams.

The observed trend is typical of activated dissociation with an onset of sticking close to 0.2 eV. At $T_n = 1100$ K, where the mean kinetic energy of H_2 is 0.22 eV, the reaction probability is 0.05%. For this T_n 70% of the reactivity is due to the dissociation of vibrationally excited molecules which account for only 0.5% in the beam. As expected, for systems with a late barrier such as H_2 + Cu, the sticking coefficients strongly depend on the rovibrational state. For the hottest beams at about 1700 K the sticking probability rises to about 7%. At this temperature, molecules in the ($v = 0$, $j = 0 - 3$) states have enough kinetic energy to account for about 50% of the beam's reactivity.

More detailed information on the dynamics of H_2 + Cu(100) is obtained in the calculated final state-resolved mean translational energies of desorption $E_{v,j}^{av}$ (Fig. 9, blue and pink colors). For each j, the $E_{v,j}^{av}$ of vibrationally excited H_2 is less than that of H_2 in the ground vibrational state. The difference $E_{0,j}^{av} - E_{1,j}^{av}$ decreases from 0.36 eV for $j = 0$–0.31 eV for $j = 7$. The reactivity of H_2 can also be enhanced by exciting the rotation of the molecule prior to the

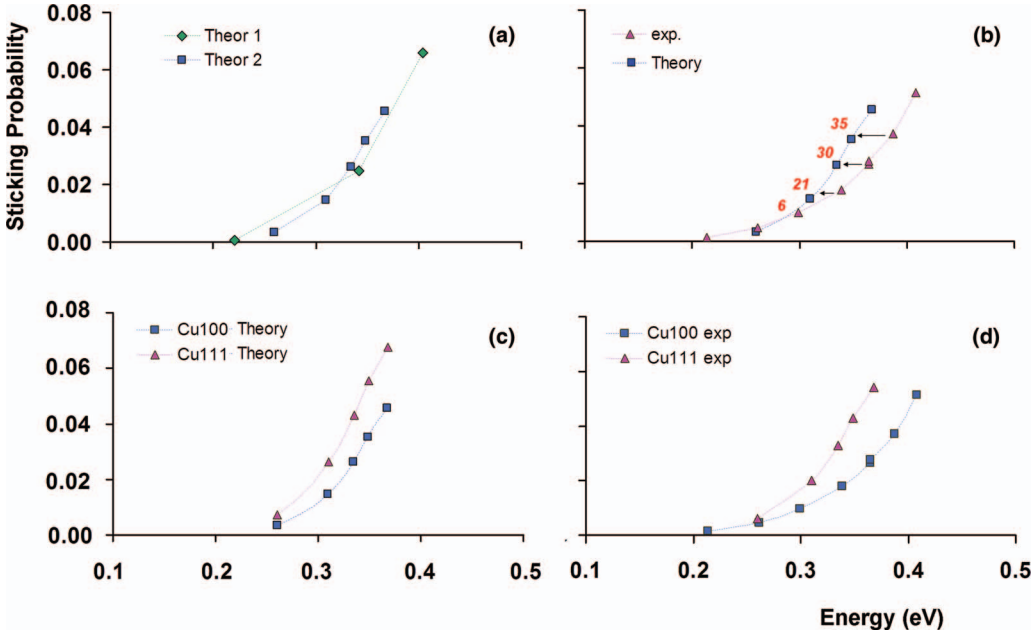

FIG. 8. Panel (a) contains the sticking probabilities computed for H_2, using the SRP functional. The theoretical results shown were based on two different methods of extracting parameters describing the molecular beams used in the experiments. The "Theor 1" theoretical reaction probabilities were obtained by averaging $R(E, T_n)$ using method 1, while method 2 was used to compute the "Theor 2" data (see Sec. S.3 of the supplementary material).[56] The sticking probabilities are shown as a function of the average translational energy in the beam. Panel (b) Reaction probabilities computed (method 1) for H_2, are compared with values measured for pure H_2 + Cu(100), labeled exp.[34,60] Arrows and the accompanying numbers, expressed in meV (1 kcal/mol = 43 meV) show the collision energy spacing between the experimental data and the cubic spline interpolated SRP-DFT reaction probability curve. In panels (c) and (d), we compare the theoretical and experimental reactivity of H_2 on Cu(100) with that on Cu(111).

collision. Figure 9 shows that for each v, the calculated mean translational energy monotonically decreases with increasing rotational quantum number. Also, for $j > 4$ the absolute values of the slopes of the curves increase with j.

2. Stereodynamics

Figure 10 shows the calculated rotational quadrupole alignment parameters for ($v = 0$, $j = 1 - 10$) H_2 and for vibrationally excited molecules with ($v = 1$, $j = 1 - 7$). For each curve the lowest energy shown is close to the translational threshold to reaction and corresponds to a total reaction probability of 1%.

All curves (Fig. 10) are completely in the positive half-plane. Accordingly, in the energy ranges considered, our calculations predict that rotational motion parallel to the surface favors the dissociation of H_2. However, the value of the alignment parameter depends strongly on both the translational energy and the rotational state j. Near the reaction threshold the $A^{(2)}_{0,v\,j}$ of vibrationally excited H_2 increases with increasing j for $2 \le j \le 6$, but the alignment parameter does not take on the maximum possible value for any value of j. For instance, ($v = 1$, $j = 7$) H_2 shows a maximum alignment parameter 70 meV above the threshold, but the value (≈ 1.1) is much smaller than the maximum possible value (1.625).

For H_2 in the ground vibrational state, the alignment at the translational energy threshold increases with increasing j for $j \ge 3$. For both the $v = 0$ and 1 vibrational state, at low

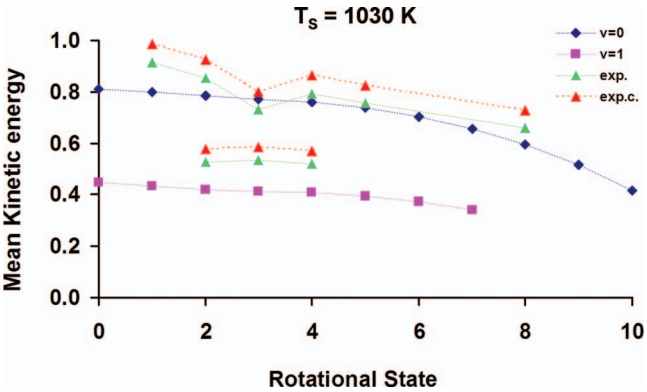

FIG. 9. Calculated (blue and pink spots) and experimental (green and red spots) average desorption energies versus rotational state at a surface temperature of 1030 K. In the legend, exp.c. refers to experimental results corrected to account for the static surface used in the calculations (see Sec. S.2 of the supplementary material).[56]

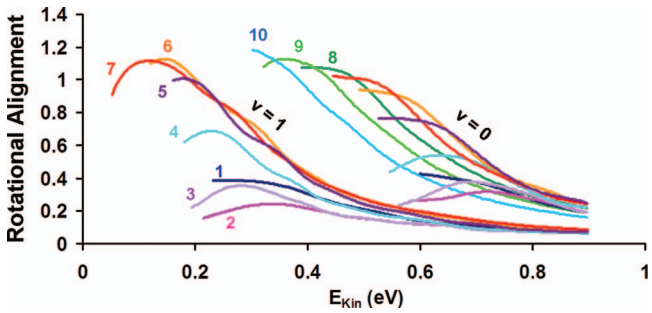

FIG. 10. Calculated rotational quadrupole alignment parameter for ($v = 0$, $j = 1 - 10$) H_2 (right side) and ($v = 1$, $j = 1 - 7$) H_2 (left side).

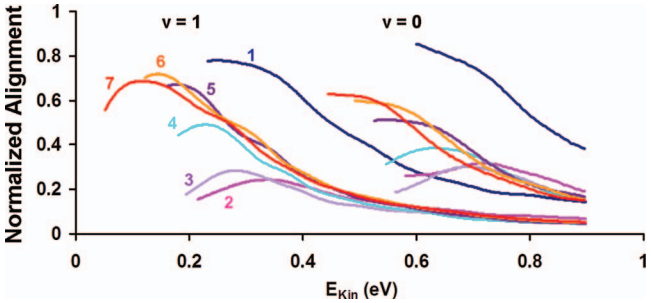

FIG. 11. Rotational quadrupole alignment parameter normalized to the maximum possible value at each j for ($v = 0$, $j = 1 - 7$) H_2 (right side) and ($v = 1$, $j = 1 - 7$) H_2 (left side). Different colors indicate different rotational states.

translational energy the quadrupole alignment increases most rapidly with j between $j = 2$ and 5, and the alignment parameter of the slowest rotating molecules ($j = 1$) is greater than or equal to that of ($j = 2$, 3) H_2. The special behavior of ($j = 1$) H_2 is even more clearly visible if one plots the "normalized" rotational alignment. For each (v, j) state considered, Fig. 11 shows the rotational quadruple alignment relative to its maximum value $3\,j/(j+1)-1$. This is a measure of how effective aligning the molecular axis can be for promoting dissociation. It is interesting to note that, for each vibrational state and especially at high translational energy, the curves for rotationally excited molecules are highly similar, except for $j = 1$ which shows a much higher normalized rotational alignment parameter.

At about 100 meV above the reaction threshold an increase of the translational energy always leads to a reduced rotational alignment parameter. The alignment parameters monotonically decrease with increasing desorption energy and slowly approach the same low limiting value, indicating a reduced preference for helicopter reaction.

3. Scattering

Figure 12 shows computed probabilities of rovibrationally (in)elastic scattering of ($v = 1$, $j = 1$) H_2. The scattering is almost totally elastic up to about 65 meV (see upper panel), after which the survival probability $P(v = 1, j = 1 \rightarrow v' = 1, j' = 1)$ monotonically decreases, reaching a value of 0.68 at 200 meV. Rotational excitation takes place mostly from $j = 1$ to $j' = 3$ (Fig. 12(a)). This transition becomes feasible when H_2 has a translational energy of about 70 meV. At 200 meV the amount of rotational excitation has increased to 20%. For scattering to the ($v' = 1$, $j' = 5$) state, ($v = 1$, $j = 1$) H_2 needs about 182 meV. At 200 meV only 0.03% of ($v = 1$, $j = 1$) H_2 ends up in the ($v' = 1$, $j' = 5$) state.

Probabilities for rovibrationally inelastic scattering to the ($v' = 0$, $j'_{odd} = 1 - 7$) states are shown in Fig. 12(b). For each state, the probability monotonically increases with the translation energy. The total probability for vibrationally inelastic scattering is about 0.1% at 70 meV, rising up to 11% at 200 meV. At low incident energies, the transitions to the ($v' = 0$, $j' = 3$) and ($v' = 0$, $j' = 5$) states are more probable than to the other ($v' = 0$, j') states, accounting for more

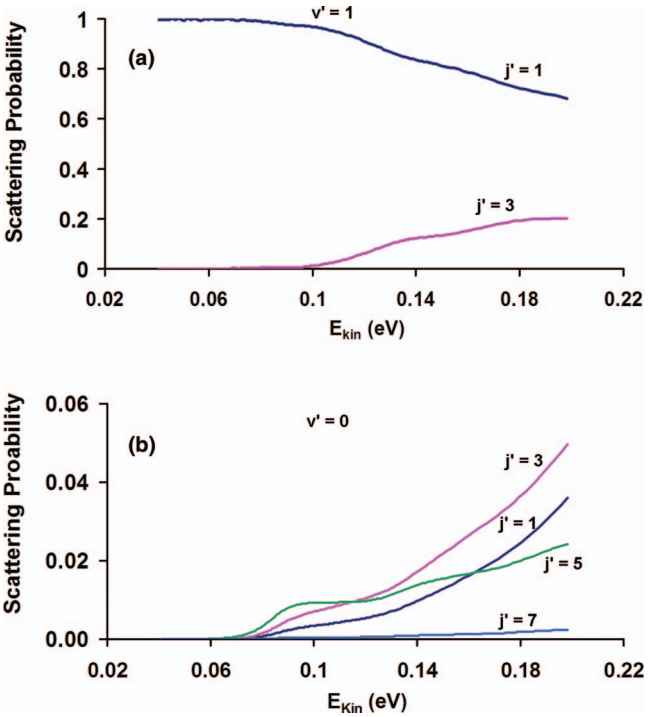

FIG. 12. Results of the calculations performed for scattering of ($v = 1$, $j = 1$) H_2. Plot (a) shows the survival probability, $P_{v=1,j=1\rightarrow v'=1,j'=1}(E)$ as well as the probability of rotational excitation, $P_{v=1,j=1\rightarrow v'=1,j'=3}(E)$ and $P_{v=1,j=1\rightarrow v'=1,j'=5}(E)$. In (b) probabilities are given for scattering into various ($v' = 0$, j') states.

than 80% of the rovibrationally inelastic scattering at 80 meV. Beyond 100 meV the scattering probability into the ($v' = 0$, $j' = 3$) state increases the fastest and reaches 5.0% at 200 meV. At this energy, the probability of vibrational deexcitation into the ($v' = 0$, $j' = 1$) state is 3.6% and it is 1.5 times the fraction of molecules deexcited into the ($v' = 0$, $j' = 5$) state. Even though the initial state internal energy is close to that of ($v' = 0$, $j' = 7$) H_2, the probability of scattering into the latter state is more than three orders of magnitude smaller than that for rovibrationally elastic scattering. The transition into ($v' = 0$, $j' = 9$) is endothermic by only 72 meV, however, the associated probability is only about 0.001 at 200 meV.

Figure 13 shows probabilities of rovibrationally (in)elastic scattering of ($v = 1$, $j = 2$) D_2. According to our calculations the dissociation probability of D_2 is zero in this range of collision energies. Unlike H_2, the scattering from the surface for the heavier D_2 molecule has an inelastic contribution already at 40 meV. At this energy the survival probability is 94% (Fig. 13(a)). Most of the rovibrationally inelastic scattering is to the ($v' = 1$, $j' = 0$) state at the low energies. At 200 meV, the probability of elastic scattering has decreased to about 63%. The probability of rotational de-excitation is only 11%. At this energy D_2 molecules also have enough energy to be rotationally excited into the ($v' = 1$, $j' = 4$) state. This transition is endothermic by about 48 meV and the calculated probability for scattering to this state monotonically increases from 0.1% to 23% over a range of incident energies from 60 to 200 meV. There is little scattering to higher rotationally excited states. The scattering

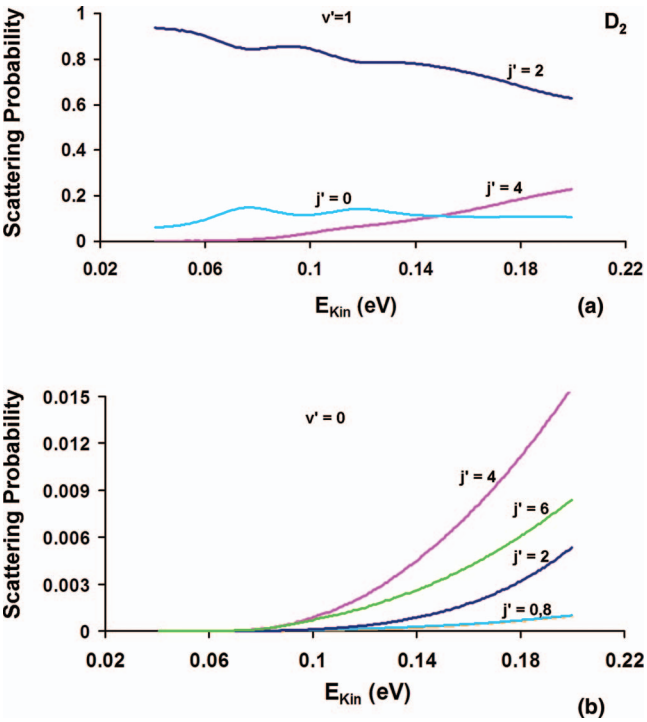

FIG. 13. Results of calculations performed for scattering of ($v = 1$, $j = 2$) D_2. The survival probability, $P_{v=1,j=2\rightarrow v'=1,j'=2}(E)$ as well as the probabilities of rotationally inelastic scattering, $P_{v=1,j=2\rightarrow v'=1,j'=0}(E)$ and $P_{v=1,j=2\rightarrow v'=1,j'=4}(E)$ are shown as a function of the collision energy (a). Probabilities for vibrationally inelastic scattering into various ($v' = 0$, j') states are also shown (b).

to ($v' = 1$, $j' = 6$) shows a threshold at 123 meV, and the probability does not exceed 0.7% at 200 meV.

Probabilities for rovibrationally inelastic scattering to ($v' = 0$, $j'_{even} = 0 - 8$) states are shown in Fig. 13(b). For each state, the probability monotonically increases with the collision energy. The total amount of rovibrationally inelastic scattering is 0.01% at 80 meV and rises up to 3.0% at 200 meV. At each collision energy, about 80% of the vibrationally inelastic scattering is to the ($v' = 0$, $j' = 4$) and ($v' = 0$, $j' = 6$) states. The transition from ($v = 1$, $j = 2$) into ($v' = 0$, $j' = 2$) involves a larger loss of internal energy and as a result the calculated probability increases from only 0.01% at 110 meV to no more than 0.50% at 200 meV. The probabilities for the transitions to ($v' = 0$, $j' = 0, 8, 10$) states are likewise small, being below 0.2%. It is interesting to note that even though the energy difference between the initial state and the ($v' = 0$, $j' = 10$) state is just 12 meV, the transition probability to this state is more than five orders of magnitude less than the survival probability.

IV. DISCUSSION

A. Reaction

Figure 9(b) compares calculated and experimental sticking probabilities,[34,60] using the experimental results of Figure 5.3 of Ref. 60. When first publishing their results for H_2 + Cu(100), Anger *et al.*[34] assumed that for $T_n > 600$ K the average translational energy of the pure H_2 beams used was well described by 2.7 kT_n. Berger[60] later performed actual measurements on TOF distributions of H_2 beams similar to the ones used in Ref. 34, and noting that the average translational energies were better described with 2.5 kT_n, he replotted the data of Figure 1 of Ref. 34 in Figure 5.3 of Ref. 60 while rescaling the collision energies by a factor 2.5/2.7.[61,62] There is excellent agreement between the theoretical and experimental probability below 300 meV. Both the calculated data and Anger's data indicate a threshold of about 0.2 eV. For averaged translational energies higher than 0.3 eV, the theoretical sticking probability increases somewhat faster than the experimental one. However, the agreement is within chemical accuracy: the theoretical results are displaced by less than 43 meV (1 kcal/mol) from the measured sticking probability curve.

The slope in the sticking probability is largely determined by the distribution of the barrier heights for dissociative adsorption in the multidimensional PES.[63,18,64] The level of agreement reached indicates that the PES describes the corrugation and the anisotropy of the reaction barrier heights rather accurately and supports assumptions made in the SRP-DFT procedure used to generate the PES. The good agreement also strongly suggests that SRP density functionals derived for H_2 interacting with a low index surface of a specific metal will also yield a good description of H_2 interacting with other low index surfaces of that metal. Furthermore, a comparison between the rescaled data of Anger *et al.*[34] for H_2 + Cu(111) and Berger *et al.*[62] for the same system suggest that even the expression $E_{av}^{kin} = 2.5\ kT_n$ may somewhat overestimate the average translational energy of pure H_2 beams for nozzle temperatures greater than 1990 K, or that the earlier measurements somehow underestimated the reaction probability for these nozzle temperatures. This suggests that the experimental results presented in Fig. 9(b) for collision energies greater than 0.33 eV should be shifted to lower energies by 12–24 meV, leading to better agreement between theory and experiment. The overall outcome is that the comparison of the sticking probabilities suggests that the reaction barrier heights in the PES are too low by 10–20 meV. This conclusion is similar to the conclusion that can be derived from the comparison between SRP-DFT theory and molecular beam sticking experiments on H_2 + Cu(111): Figure 2B of Ref. 18 suggests that the barriers in the SRP-DFT PES for this system are too low by 10–30 meV.

Panel (c) of Fig. 9 compares the theoretical sticking curves for a beam of H_2 on the Cu(100) and Cu(111) surfaces. In addition, Fig. 9(d) shows the experimental results. According to the dynamical calculations the (111) surface of copper is slightly more reactive towards H_2 than the (100) surface in the energy range considered. The experimental curves show a similar trend. Our results also agree well with the theoretical predictions stated in Ref. 65 which attributed the greater reactivity of the Cu(111) face to lower barrier heights on this surface, which could be only partially compensated by the greater vibrationally efficacy for H_2 on Cu(100). This interpretation agrees with our SRP-DFT results; for instance, on the (111) face the minimum (bridge-to-hollow) barrier height (0.63 eV[18]) is lower than on Cu(100) (0.74 eV, see Table I).

In order to analyze the effect of the initial rovibrational state on the reactivity, we compare theoretical ADEs with experimental values in Fig. 8. The SRP results reproduce the experimental data fairly well, with maximum absolute errors of 91 meV for ($v = 0$) H_2 and 110 meV for ($v = 1$) H_2. However, this comparison of experimental results for $T_s = 1030$ K with static surface computational results did not yet take into account that the experimental mean desorption energies have to be increased to account for the use of an effectively low surface temperature (0 K) in the theory, which results in reaction probability curves with too low width, and therefore in a higher average desorption energy (see Sec. S.3 of the supplementary material).[56] Making this correction, the maximum error increases to about 160 meV both for ($v = 0$) H_2 and ($v = 1$) H_2 with respect to experimental results which have been corrected for surface temperature effects[66] to take into account that the calculations have been performed on a static surface (red values in Fig. 8). The theoretical results tend to be lower than the experimental average desorption energies, whereas for H_2 + Cu(111) theoretical values based on SRP-DFT tended to be higher than the experimental desorption energies.[24]

To understand the above described discrepancy in the comparison between experimental and theoretical results for state-resolved average desorption energies for H_2 + Cu(111) and H_2 + Cu(100), we have compared the new results for Cu(100) ($T_s = 1030$ K) and the previous results for Cu(111)[66] (based on measurements performed at $T_s = 925$ K) to the previous results of Comsa and David,[33] who reported state-averaged average desorption energies for $T_s = 1000$ K for both low index Cu surfaces. The state-averaged results of Comsa and David[33] should be the most accurate because they used a far longer flight path in their TOF measurements than used in the present experiments on Cu(100) and in the previous measurements on Cu(111).[66] Measured and computed (with SRP-DFT dynamics) values are collected in Table II. Comsa and David[33] reported rather precise values for D_2 in their Figure 3(b), but simply listed the H_2 values as 8 kT_s in their abstract. For this reason, we also report estimates of their values for H_2 as the values they measured for D_2 – 30 meV, with the 30 meV correction coming from computed quasi-classical values for H_2 and D_2 + Cu(111) differing by 30 meV, with the D_2 value being slightly higher.[67,24] In Table II, we compare the Comsa and David[33] values we computed for H_2 (in range 0.60–0.69 eV) with the value extracted for H_2 + Cu(111) from fits to initial state-resolved reaction probabilities to the data of Rettner *et al.*[66] (0.56 eV, note that Michelsen *et al.*[68] report a possible error up to 10% in absolute values of average desorption energies in their related work on D_2 + Cu(111)) and with the value obtained experimentally in the present work for H_2 + Cu(100) (0.76 ± 0.05 eV, with the large uncertainty coming mostly from the $v = 1/v = 0$ population ratio in desorption).

The present comparison suggests that the experimental state-resolved desorption energies measured by Rettner *et al.*[66] for H_2 + Cu(111) may underestimate the true values by about 10%, whereas the values measured here for H_2 + Cu(100) may overestimate the true values by the same amount.

In Table II, we also included the quantum dynamics result obtained here with the SRP-DFT PES for H_2 + Cu(100) for a static surface (0 K), and the estimated value for $T_s = 1000$ K obtained by subtracting 50 meV from the static surface result. These values are in good agreement with the values obtained by Comsa and David[33] (Table II). However, the comparison of our theory for H_2 + Cu(100) to molecular beam sticking experiments that is presented above would suggest that our computed average desorption energy for H_2 + Cu(100) could be too low by 30–40 meV. The above discussion explains why previously computed SRP-DFT state-resolved desorption energies seemed to overestimate experimental values for H_2 + Cu(111),[24] whereas the present computed SRP-DFT state-resolved desorption energies would seem to underestimate the experimental values for H_2 + Cu(100).

The results in Fig. 8 clearly show that vibrationally exciting the molecule enhances its reactivity. The presence of a late barrier may also lead to adiabatic rotational-translational energy transfer, due to the lowering of the rotational constant as the molecule travels along the reaction path.[69] For H_2 in the ground vibrational state, increasing j from $j = 1$ to $j = 8$ the ADE decreases by 250 meV for the experimental data; similar behavior is obtained in the theory, where the ADE decreases by 210 meV.

B. Stereodynamics of reaction

In Figs. 14 and 15, theoretical rotational quadrupole alignment parameters are compared with experimental

TABLE II. Experimental and computed state-averaged average desorption energies (eV), for dihydrogen desorbing normal to the surface at a surface temperature of 1000 K from Cu(100) and Cu(111), QC are quasi-classical and QD are quantum dynamical results. See also the text for further explanations.

	Cu(111)	Cu(100)
D_2, C&D exp. (from text and Fig. 3(b) of Ref. 33)	0.63	0.68
H_2, C&D exp. (from abstract " = 8kT$_s$" of Ref. 33)	0.69	0.69
H_2, C&D exp. (est[a] from D_2 value[33] + calcs)	0.60	0.65
H_2, RM&A exp., computed from exp. fits	0.56 (Ref. 66)	
H_2, computed with QD, SRP-DFT (0 K)	0.67 (Refs. 67 and 24)	0.72
H_2, computed with QD, SRP-DFT (1000 K, est.[b])	0.62 (Refs. 67 and 24)	0.67
H_2, exp. (this work)		0.76 ± 0.05

[a]Estimated from $\langle E\rangle_{D_2}^{100} \approx \langle E\rangle_{H_2}^{100} + \langle E\rangle_{D_2}^{111} - \langle E\rangle_{H_2}^{111}$, using SRP-DFT computed values for the latter two quantities as calculated using quasi-classical dynamics.

[b]50 meV subtracted to account for higher surface temperature.

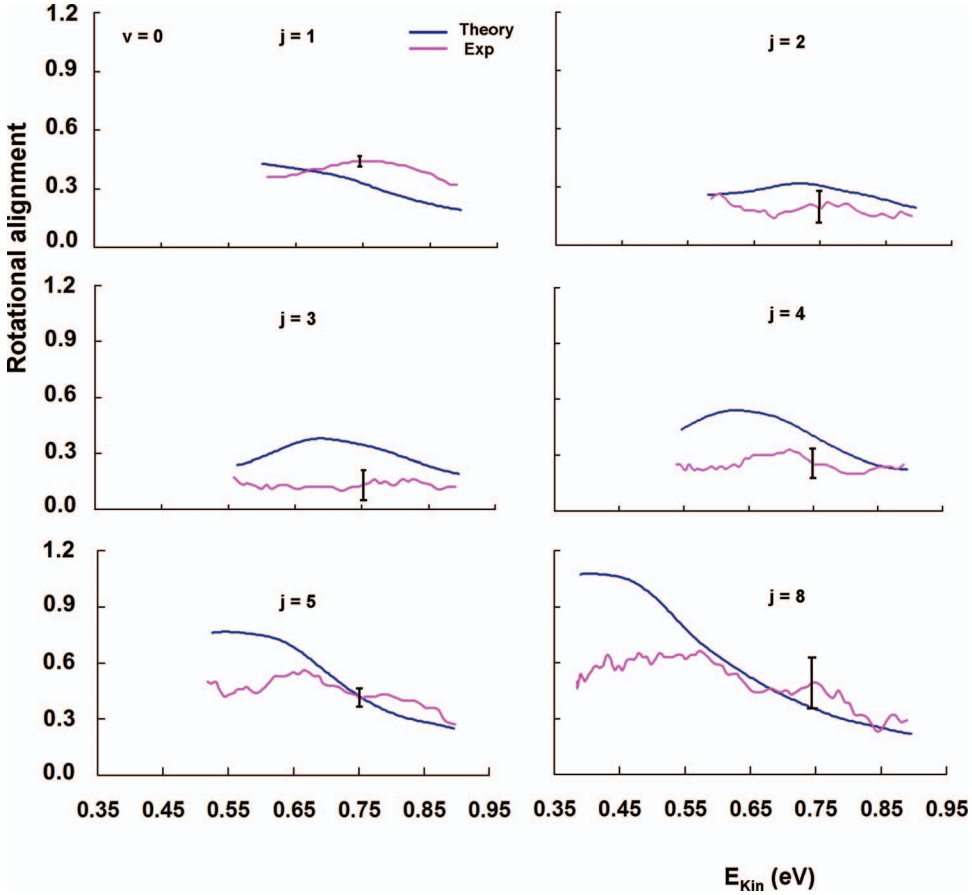

FIG. 14. Theoretical and experimental quadrupole alignment parameters for different ($v = 0$, j) H_2.

values. For each curve the lowest energy shown is close to the computed translational threshold to reaction, which corresponds to a total reaction probability of 1%. Computed sticking probabilities increase with translational energy, suggesting that numerical noise should not much affect the reliability of the computed quadrupole alignment parameters for energies greater than the translational thresholds defined above.

For H_2 in the vibrational ground state (Fig. 14), the agreement between theory and experiment seems best for slow rotating molecules. For ($v = 0$, $j = 1, 2$) H_2, the maximum difference between theory and experiments is, respectively, 0.18 and 0.13. In the energy range considered, the experimental alignment parameters for H_2 in the states ($v = 0$, $j = 3, 4$) are quite flat as opposed to the theoretical curves, which have a broad maximum at about 0.65 eV. The largest difference between theory and experiments is about 0.25 and decreases to 0.1 above 0.8 eV. For ($v = 0$, $j = 5$) H_2, the difference between the curves in Fig. 14 has a maximum of 0.3 at the reaction threshold, and then decreases to less than 0.1 at about 0.7 eV. For ($v = 0$, $j = 8$) H_2, theoretical and experimental data are in good agreement above 0.55 eV, but near the reaction threshold the computed alignment parameter is about twice the experimental value. For most ($v = 0$, j) states and at most translational energies, the theoretical alignment parameters are larger than the experimental values, in agreement with earlier static SRP-DFT results for ($v = 0$, $j = 11$) D_2 desorbing from Cu(111).[24] As argued also for this system[24] for D_2 + Cu(111) and later demonstrated for this system with AIMD calculations,[19] part of the disagreement could be due to the static surface approximation: the computed alignment parameter would be expected to be lowered on a temperature roughened surface also for the H_2 + Cu(100) system studied here, leading to better overall agreement with experiment for $v = 0$ H_2 + Cu(100).

If one also considers the normalized rotational alignments shown in Fig. 11, three different features are clearly visible in both the theoretical end experimental data: (i) for all the j values, the rotational quadrupole alignment parameters never reach their maximum limiting values, (ii) the alignment of the molecular axis nevertheless strongly influences the dissociation of ($v = 0$, $j = 1$) H_2, especially at low translational energy, and (iii) near the threshold the $A^{(2)}_{0,v\,j}$ curve for ($v = 0$, $j = 1$) H_2 is higher than the curves for ($v = 0$, $j = 2, 3$) H_2, which are almost superimposed, but for higher values of j at threshold $A^{(2)}_{0,v\,j}$ increases with j.

The behavior of the curves can be rationalized considering that the rotational energy can both hinder (steric hindering effect) and enhance (rotational enhancement effect) H_2 dissociation on metal surfaces. As discussed in Ref. 46, the steric hindering effects can be divided into two separate mechanisms. The first is orientational hindering and the second rotational hindering. Both hindering effects are a result of the anisotropy of the molecule-surface interaction, which describes the effect that the molecule must be parallel to the

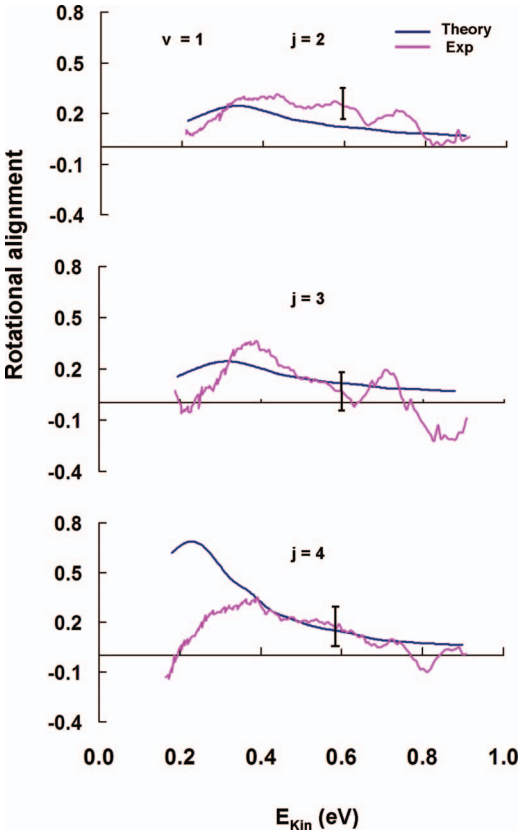

FIG. 15. Theoretical and experimental quadrupole alignment parameters for different $(v = 1, j = 2 - 4)H_2$.

surface to facilitate the attractive orbital overlap leading to dissociation. Rotational hindering is also a dynamical effect: Molecules rotating too fast may encounter an unfavorable orientation while travelling along the bottleneck of the reaction path (the barrier region), regardless of the initial orientation of the molecule. If a high anisotropy is present in the neighborhood of the barrier, this may of course lead to reflection. In contrast, pure orientational hindering refers to a static effect: Non-rotating or slow-rotating molecules will be reflected from an anisotropic barrier if their initial orientation is unfavorable.

Rotation may hinder the reaction, but it can also help molecules to react. Rotational enhancement effects can also occur by two different mechanisms. In the first mechanism, rotation enhances the reaction due to the decrease of the molecule's rotational constant as it approaches a late barrier. In fact near the barrier the molecular bond is stretched. This stretching increases the moment of inertia and decreases the rotational energy associated with the rotational state j. Assuming that the dissociation occurs without change in the rotational quantum state, this should lead to an adiabatic energy transfer from the rotation to the translation along the reaction path. For this mechanism, which has been called elastic rotational enhancement,[46] the higher the j level is, the more rotational energy can be transferred into motion towards the barrier. Elastic rotational enhancement will equally enhance reaction of cartwheels and helicopters, of a given j level, and it should therefore have a less direct influence on the rotational alignment parameter of the reacting molecules.

The second mechanism of enhancement is closely related to the potential anisotropy in ϑ near the barrier. Not only will a high anisotropy induce hindering effects, as explained above, it may also allow the molecule to rotationally deexcite on its way to the barrier and thereby help the reaction. The energy gained from this de-excitation can be transferred into motion along the reaction path and thereby help the molecule to cross the barrier. Due to the inversion symmetry of H_2, this mechanism can only be effective for molecules with $j \geq 2$. In addition, its effectiveness is very dependent on the specific level (j, m_j) of H_2. Specifically, j should be larger than 1, but not too large because that leads to large energy gaps with the states to which de-excitation takes place. Furthermore, because rotationally inelastic transitions are to a large extent m_j conserving and a de-excitation has to take place, the mechanism is favored for molecules with small absolute m_j values, and should thereby contribute to a lowered alignment. This mechanism of rotational enhancement is referred to as inelastic rotational enhancement.[46] It is expected to be especially important near threshold, where reaction may only be possible through this mechanism.

For energies above the threshold, the rotational alignments are positive reflecting the fact that hydrogen molecules more easily dissociate if their axis is parallel to the surface, due to the enhanced overlap of the $2\sigma^*$ orbital with the metal orbitals. With increasing translational energy reaction becomes possible for an increasing number of orientations, explaining the general trend that at high translational energy the alignment decreases with translational energy.[70]

For H_2 in the $(v = 0, j = 1)$ state no rotational de-excitation is possible because for H_2 the change in j must be even. Because rotationally inelastic enhancement cannot lead to a decreased alignment parameter for this state, the normalized rotational alignment parameter for this state is quite high (see Fig. 11). For H_2 with j somewhat higher than one, near the threshold dissociation of cartwheel molecules rises due to the energy released through the rotationally inelastic mechanism. This explains why, at low translational energy, even the unnormalised rotational alignment parameter curve is lower for $j = 2$ than for $j = 1$, in both the theory and the experiment (see also Fig. 16 which clearly shows this trend). As explained above and further in Ref. 46 rotationally inelastic enhancement should become less effective again at some point for $j > 2$, explaining why the alignment curves start to rise with j again for $j > 2$ (in the theory) or 3 (in the experiment).

Figure 16 clearly shows the trend that, especially at low translational energy, the rotational alignment parameter first decreases with j, and then increases again, in both the theory and in the experiment. There are differences in the details: in the theory, the lowest alignment parameter is found for $j = 2$, except at the lowest translational energy, where the alignment parameter for $j = 3$ is lowest, whereas in the experiment the $j = 3$ alignment parameter is lowest for all translational energies. However, the overall trend is the same and emphasizes the importance of rotationally inelastic enhancement, which promotes reaction of states with j small but larger than 1, and small $|m_j|$[46] near the threshold to reaction.

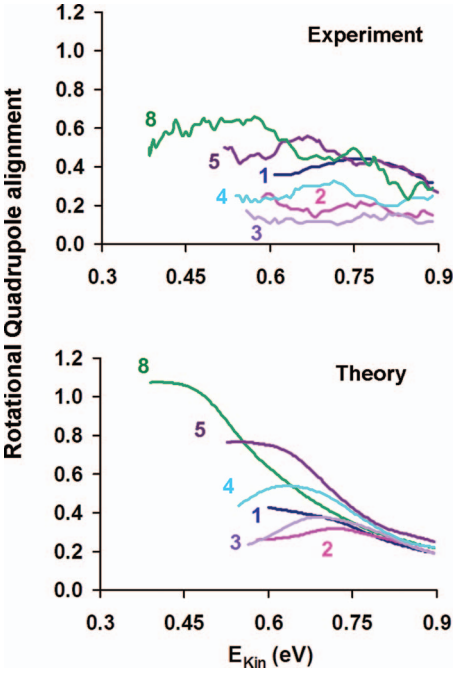

FIG. 16. The rotational alignment parameter is shown for ($v = 0, j = 1$–5 and 8), as a function of translational energy, for translational energies at which the degeneracy averaged reaction probability exceeds 0.01. (Upper panel) Experimental results. (Lower panel) Theoretical results.

Figure 15 shows a comparison between the calculated and the experimental alignment curves for H_2 in the ($v = 1$, $j = 2 - 4$) states. There is quite good agreement between theory and experiment in the range 400–800 meV. In this range, both calculated and empirical alignment data are in the positive half-plane indicating a larger reactivity of molecules with their angular momentum vector perpendicular to the surface. For ($v = 1$, $j = 2, 3$) H_2, the agreement remains good also below 400 meV. The two theoretical curves have a broad maximum at about 350 meV, which slightly differs in height and position from the maxima in the experimental alignments. For ($v = 1$, $j = 4$) H_2, the calculated curve has a maximum near the reaction threshold, where the experimental quadrupole alignment is approximately zero; the experimental curve reaches its maximum only around 400 meV. The panels of Fig. 15 show further that the height of the experimental peaks does not seem affected much by the variation of the rotational quantum number, being approximately 0.35. In contrast, the theoretical peak height depends more strongly on j.

C. Rovibrationally (in)elastic scattering

Figure 17 shows a comparison between theoretical and experimental[16] rovibrationally (in)elastic scattering probabilities for H_2. Panel (a) shows the survival probability of ($v = 1$, $j = 1$) H_2.

Both theoretical and experimental data show a decrease in the survival probability with increasing translational energy, however, in the whole range considered the quantum dynamical calculations always overestimate the experimental data, by about 0.35 on average. Our calculations indicate that the scattering of H_2 on Cu(100) is almost totally elastic below 65 meV, whereas the measured rovibrationally elastic scattering probability is only about 65% at 0.06 eV.

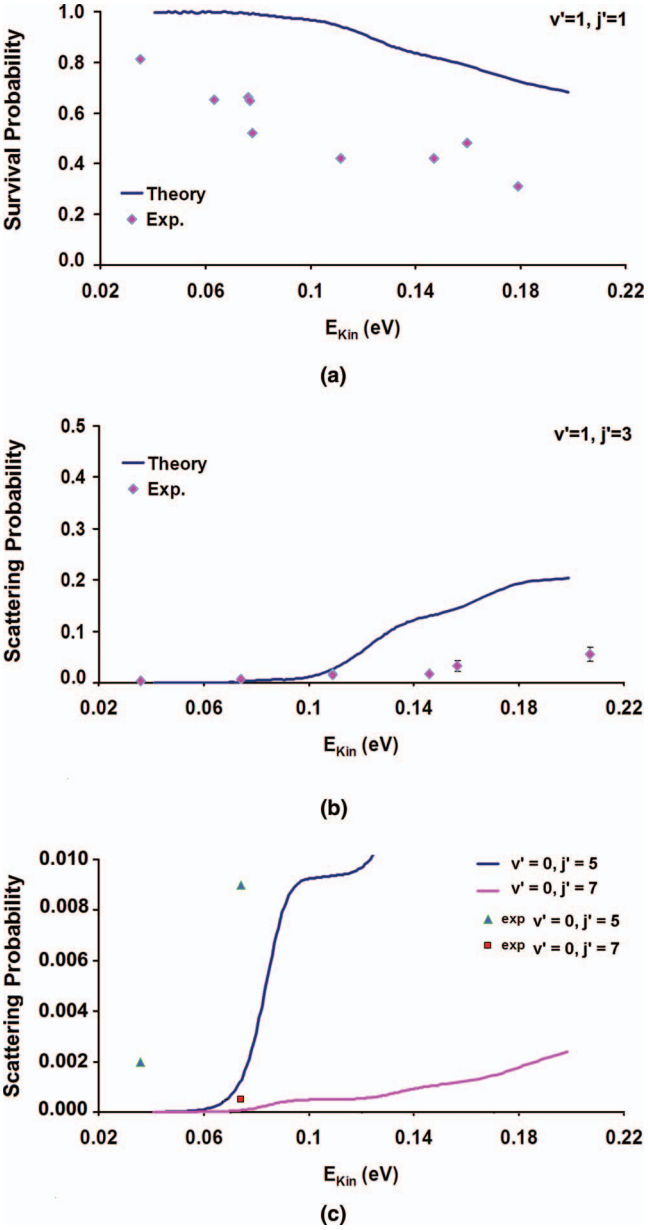

FIG. 17. Theoretical probabilities for rovibrationally (in)elastic scattering of H_2 ($v = 1$, $j = 1$) are compared with experimental values. Plot (a) shows the survival probability, $P_{v=1,j=1\to v'=1,j'=1}(E)$; panel (b) contains the probability of rotational excitation $P_{v=1,j=1\to v'=1,j'=3}(E)$. In (c) probabilities are given for scattering into ($v' = 0$, $j' = 5, 7$) states.

Figure 17(b) shows the calculated and experimental probabilities for rotational excitation of H_2 from the initial ($v = 1$, $j = 1$) state into the ($v' = 1$, $j' = 3$) state. The experimental data show that the probability of rotationally inelastic scattering increases from 0.35% at 36 meV to 5% at 206 meV. Even though the rotational excitation is endothermic by about 70 meV, a threshold is not clearly visible. At 74 meV the measured excitation probability is 0.7%. The theoretical curve in Fig. 17(b) shows a threshold very close to

TABLE III. Experimental rovibrationally inelastic scattering probabilities are compared to calculated SRP-DFT scattering probabilities.

Isotopomer	Initial state	Final state	E_{coll} (meV)	Theory	Exp.
D_2	$v = 1, j = 2$	$v = 0, j = 6$	78	0.00004	< 0.002
D_2	$v = 1, j = 2$	$v = 0, j = 6$	199	0.0066	< 0.003
H_2	$v = 1, j = 1$	$v = 0, j = 5$	36	0.00001	0.002
H_2	$v = 1, j = 1$	$v = 0, j = 5$	74	0.0014	0.009
H_2	$v = 1, j = 1$	$v = 0, j = 7$	74	0.0001	0.0005

67 meV in accordance with the Born-Oppenheimer static surface model used. Once the kinetic energy reaches the value of 74 meV, the theoretical probability is 0.29%. At 110 meV the difference between theory and experiment is about 0.012, but at higher energies the difference P(Theory)−P(Exp.) rapidly increases with collision energy, reaching a value of about 0.11 at 150 meV. At 206 meV the calculated probability is about 2.8 times higher than the experimental one.

Previous dynamics simulations obtained on a Becke-Perdew GGA PES (PES5)[45] gave probabilities for rotationally inelastic scattering at least seven times larger than the experimental results in the energy range considered. The present results indicate that the SRP procedure used to generate the PES has improved the agreement between theory and experiment, but the agreement is still far from quantitative. Here, it should be noted that probabilities for rotationally inelastic scattering are quite sensitive to the detailed features of the PES.[71] However, for H_2 + Cu(111) SRP-DFT based theory gave a chemically accurate description of the ratio of the probability of rotational excitation from $j = 0$ to $j = 2$ divided by the probability for rotationally elastic scattering, both from the ($v = 1$, $j = 0$) state.[18] It is not clear why similarly good agreement is not achieved here for H_2 ($v = 1$, $j = 1$) scattering rotationally (in)elastically from Cu(100).

Figure 17(c) shows that the experimental probability for relaxation into ($v' = 0$, $j' = 5$) increases from 0.002 at 36 meV to 0.009 at about 74 meV (see also Table III). Furthermore, according to Watts and Sitz[16] the probability of rovibrationally inelastic scattering to ($v' = 0$, $j' = 7$) was 0.0005 at 74 meV, and too small to be measurable at 36 meV. According to theory, the probability of scattering into ($v' = 0$, $j' = 5$) state is of the order of 10^{-6} at 40 meV, increasing to 0.009 at 94 meV (Table III). At this energy the computed $P(v = 1, j = 1 \rightarrow v' = 0, j' = 7)$ H_2 is 0.00045. Theoretical and experimental results agree on several aspects: at low collision energies relaxation to ($v' = 0$, $j' = 5, 7$) is a minor channel, with $P(v = 1, j = 1 \rightarrow v' = 0, j' = 7)$ being more than three orders of magnitude smaller than the probability for elastic scattering: $P(v = 1, j = 1 \rightarrow v' = 0, j' = 7)$ is about 20 times smaller than $P(v = 1, j = 1 \rightarrow v' = 0, j' = 5)$ above 70 meV. Comparing to previous theoretical results for H_2 + Cu(100) obtained on a Becke-Perdew DFT PES,[45] for vibrational inelastic scattering the SRP DFT approach substantially improves the agreement with the experiments, as is the case for rotationally inelastic scattering.

In Fig. 18, the theoretical calculations performed for scattering of ($v = 1$, $j = 2$) D_2 are compared with experiments.

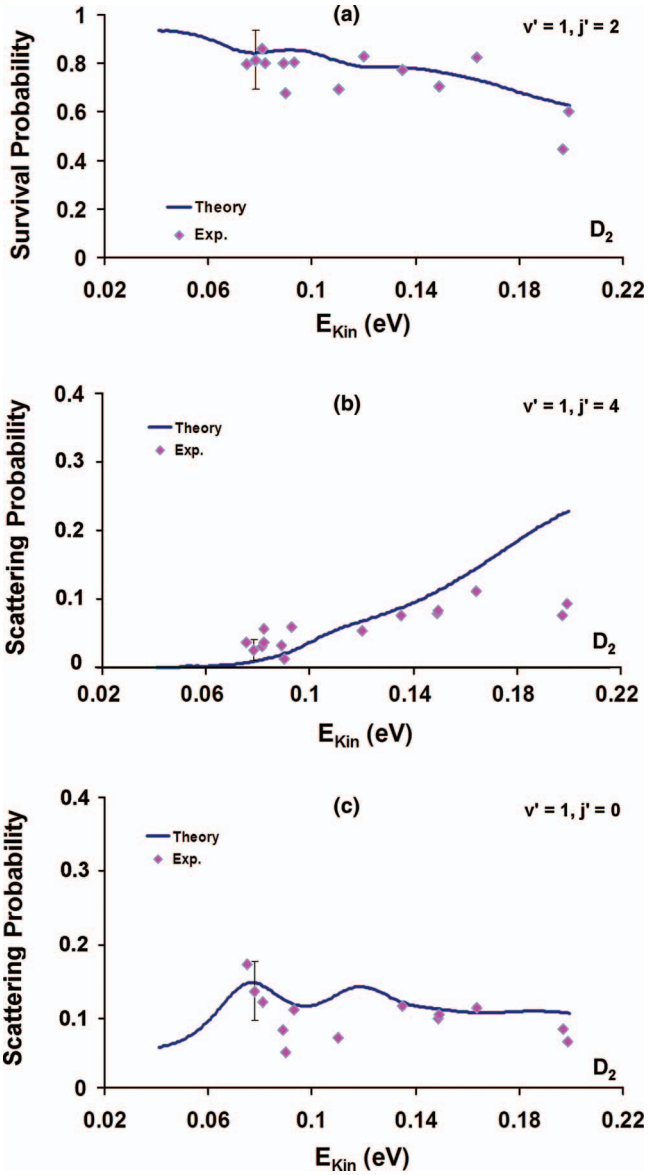

FIG. 18. Theoretical and experimental scattering probabilities of D_2 ($v = 1$, $j = 2$) are compared. Shown are (a) the survival probability, (b) the probability of rotational excitation into the ($v' = 1$, $j' = 4$) state, and (c) the probability of rotational de-excitation into ($v' = 1$, $j' = 0$).

Panel (a) shows very good agreement between survival probabilities measured by Shackman and Sitz[17] and the new theoretical results obtained with SRP-DFT. According to the experiments, for an incident energy of 79.0 ± 0.6 meV, the survival probability is 0.81 ± 0.12. The theoretical probability at the same incident energy is 0.84. For scattering of ($v = 1$, $j = 2$) D_2 from Cu(100), Shackman and Sitz[17] only presented error bars in their rotationally (in)elastic scattering probabilities for one value of the collision energy, which can be taken as indicative of the size of the experimental error bars over the entire energy range for which experimental results were obtained.[72] Using this information, we see that the SRP-DFT results for rotationally elastic scattering agree with the experimental results within experimental error for almost all energies.

Panel (b) of Fig. 18 contains the $P(v = 1, j = 2 \rightarrow v' = 1, j' = 4)$. The agreement between theory and experiment is very good for energies up to 170 meV. The experimental probabilities increase from 2.5% to 11% over a range of translational energies from 80 to 170 meV. The theoretical probabilities increase from 1% to 12% in the same energy range. However, at 200 meV the calculated scattering probability (19%) is about twice the experimental value (10%).

For rotational de-excitation into $(v' = 1, j' = 0)$, the SRP probabilities rapidly increase from 5% to 10% as the incident energy increases from 40 to 80 meV (Fig. 18(c)). For higher energies, the calculated probabilities slightly oscillate to reach a value of 11% at 140 meV and then remain almost constant until 200 meV. The experimental results are strongly scattered around a probability of 10% in the range of energies considered, and for most energies the theoretical results agree with the experimental rotational de-excitation probabilities to within experimental error.

The probability of vibrational de-excitation of D_2 $(v = 1, j = 2)$ into $(v' = 0, j')$ states is very low. According to Shackman,[17] for D_2, the sum of the transition probabilities to $(v' = 1, j' = 4)$ and $(v' = 1, j' = 0)$ accounted for the missing fraction of molecules in the survival probability measurements for most of the incident energies considered. According to both our calculations and the previous experiments the transition probability of D_2 $(v = 1, j = 2)$ into $(v' = 0, j' = 6)$ is smaller than 0.002 at 78 meV (Table III). For this transition, an upper bound of 0.003 was experimentally estimated at 200 meV. At this collision energy, the SRP DFT probability is 2.2 times the upper bound derived from the experiments (Table III).

Summarizing the results for scattering, for H_2 $(v = 0, j = 1)$ theory predicts a survival probability that is about 0.35 higher than the experimental result, over the entire range of translational energies for which experimental results are available. At low collision energies, below 100 meV, theory and experiments agree on the amount of $(v = 1, j = 1)$ H_2 rotationally excited into the $(v' = 1, j' = 3)$ state and on the main aspects of vibrationally de-excitation into $(v' = 0, j' = 5, 7)$ states. Above 110 meV the SRP rotational excitation probability to $j' = 3$ is considerably larger than the experimental value. For D_2, the rotationally (in)elastic scattering probabilities computed with SRP-DFT accurately reproduce the experimental results up to 170 meV.

If the amount of rotationally inelastic scattering is a measure of the anisotropy of the PES, then the comparison of the theoretical results with the experimental results suggests that, near the barrier, the present PES somewhat overestimates the anisotropy of the molecule-surface interaction. At 200 meV, the probability of rotational excitation of H_2 (D_2) is 2.8 (1.9) times the experimental value. On the other hand, rotational de-excitation of D_2 is well described at this collision energy. Further from the barrier, in the entrance channel, the anisotropy of the PES is likely to be correct since below 100 meV the agreement with the experiments is fairly good. Our end conclusion is that the SRP-DFT approach accurately describes rotationally elastic and inelastic scattering of $(v = 1, j = 2)$ D_2 from Cu(100), whereas data on rotationally elastic and inelastic scattering of H_2 $(v = 1, j = 1)$ from the same surface, which should probe more elevated regions of the PES,[17] are less well described by SRP-DFT.

V. CONCLUSION

We have presented new experimental and theoretical results for reactive scattering of dihydrogen from Cu(100). In the new experiments, the associative desorption of H_2 has been investigated in a velocity resolved manner, using time-of-flight techniques. Rovibrational state-selectivity was achieved by detecting the desorbed H_2 with resonance-enhanced multi-photon ionization laser detection. This way, average desorption energies could be measured. By using polarised laser light, it was also possible to measure rotational quadrupole alignment parameters for H_2 $(v = 0, j = 1 - 5, 8)$ and $(v = 1, j = 2 - 4)$.

We have also performed quantum dynamics calculations based on a potential energy surface computed with a SRP density functional, which was derived earlier for dihydrogen interacting with Cu(111). These calculations were performed employing the Born-Oppenheimer static surface model. The results of the calculations have been compared with earlier molecular beam sticking experiments on H_2 + Cu(100). The calculations using the SRP density functional derived for dihydrogen interacting with Cu(111) reproduce the sticking probabilities measured for H_2 + Cu(100) with chemical accuracy. This suggests that SRP density functionals fitted to molecular beam sticking experiments on dihydrogen interacting with a particular low index face of a specific metal may be used to reproduce sticking experiments on dihydrogen reacting with another low index face of that metal, with chemical accuracy. It also suggests that the SRP functional thus developed may yield accurate results for H_2 interacting with a defected (e.g., stepped) surface of that same metal, in a system of catalytic interest.

The results of the calculations have also been compared with the results of the new experiments and with the results of previous molecular beam experiments on rovibrationally elastic and inelastic scattering of H_2 and D_2 from Cu(100). The results of these comparisons are not as unequivocal as the results of the comparison to the molecular beam sticking experiment. A highly accurate description has been obtained of rovibrationally elastic and inelastic scattering of D_2 from Cu(100), and of the orientational dependence of reaction of $(v = 1, j = 2 - 4)$ and $(v = 0, j = 1, 2)$ H_2 on Cu(100). However, the computed average desorption energies agreed less well with the new state-resolved experimental results; the theoretical average desorption energies computed for H_2 + Cu(100) were lower than the experimental values. The probabilities of rotationally elastic and inelastic scattering of H_2 $(v = 1, j = 1)$ from Cu(100) were too high compared to experiment. The static surface model results using the SRP density functional were also not yet accurate for the orientational dependence of reaction of $(v = 0, j = 3 - 5, 8)$ H_2 on Cu(100). More research is needed to establish whether more accurate SRP-DFT dynamics results can be obtained for these observables if surface atom motion is added to the dynamical model.

An interesting observation is that, at the threshold energy for reaction, the rotational quadrupole alignment parameter first decreases with j going from $j = 1$ to $j = 3$, and then increases again, in both the theory and the new experiments. This qualitative behavior had been predicted in earlier theoretical calculations on H_2 + Cu(100), which also considered rotational de-excitation.[45] The calculations suggest that it arises from a mechanism in which the reaction of low m_j states is rotationally enhanced, i.e., reaction is helped by rotational de-excitation of cartwheel-like states releasing energy to the reaction co-ordinate. Because this mechanism occurs predominantly for cartwheel states with low j, the rotational quadrupole alignment parameter is decreased for low j, with the restriction $j > 1$ arising from the nuclear spin symmetry of the molecule, which prohibits rotational de-excitation for $j < 2$.

ACKNOWLEDGMENTS

We are grateful to Cristinia Diáz for making her theoretical SRP-DFT results for state-averaged average desorption energies for H_2 and D_2 + Cu(111) available to us prior to the publication of these results. H. Zacharias acknowledges partial financial support through Deutsche Forschungsgemeinschaft (DFG) Grant No. Za 110/15.

We also thank stichting Nederlandse Computer Faciliteiten (NCF) of Nederlandse organisatie voor Wetenschappelijk Onderzoek (NWO) for an allocation of time on the Dutch national supercomputer Huygens, and Chemische wetenschappen (CW)/NWO for a TOP grant.

[1] G. A. Somorjai, *Introduction to Surface Chemistry and Catalysis* (Wiley, New York, 1994).
[2] I. Chorkendorff and J. W. Niemantsverdriet, *Concepts of Modern Catalysis and Kinetics* (Wiley-VCH Verlag GMBH, Weinheim, 2003).
[3] G. J. Kroes, Science **321**, 794–797 (2008).
[4] G. J. Kroes, Phys. Chem. Chem. Phys. **14**, 14966 (2012).
[5] L. Diekhöner, L. Hornekaer, H. Mortsensen, E. Jensen, A. Baurichter, V. V. Petrunin, and A. C. Luntz, J. Chem. Phys. **117**, 5018 (2002).
[6] J. D. White, J. Chen, D. Matsiev, D. J. Auerbach, and A. M. Wodtke, Nature (London) **433**, 503–505 (2005).
[7] N. Shenvi, S. Roy, and J. C. Tully, Science **326**, 829–832 (2009).
[8] L. Martin-Gondre, M. Alducin, G. A. Bocan, R. Diéz Muiño, and J. I. Juaristi, Phys. Rev. Lett. **108**, 096101 (2012).
[9] S. Nave and B. Jackson, Phys. Rev. Lett. **98**, 173003 (2007).
[10] J. Zheng, Y. Zhao, and D. G. Truhlar, J. Chem. Theory Comput. **5**, 808–821 (2009).
[11] R. Peverati and D. G. Truhlar, J. Phys. Chem. Lett. **3**, 117–124 (2012).
[12] D. C. Clary, Science **321**, 789–791 (2008).
[13] A. C. Luntz and M. Persson, J. Chem. Phys. **123**, 074704 (2005).
[14] J. I. Juaristi, M. Alducin, R. Diéz Muiño, H. F. Busnengo, and A. Salin, Phys. Rev. Lett. **100**, 116102 (2008).
[15] P. Nieto, E. Pijper, D. Barredo, G. Laurent, R. A. Olsen, E. J. Baerends, G. J. Kroes, and D. Farías, Science **312**, 86–89 (2006).
[16] E. Watts and G. O. Sitz, J. Chem. Phys. **114**, 4171–4179 (2001).
[17] L. C. Shackman and G. O. Sitz, J. Chem. Phys. **123**, 064712 (2005).
[18] C. Díaz, E. Pijper, R. A. Olsen, H. F. Busnengo, D. J. Auerbach, and G. J. Kroes, Science **326**, 832–834 (2009).
[19] F. Nattino, C. Díaz, B. Jackson, and G. J. Kroes, Phys. Rev. Lett. **108**, 236104 (2012).
[20] H. A. Michelsen, C. T. Rettner, and D. J. Auerbach, Surf. Sci. **272**, 65–72 (1992).
[21] M. J. Murphy and A. Hodgson, J. Chem. Phys. **108**, 4199–4211 (1998).
[22] M. Dohle and P. Saalfrank, Surf. Sci. **373**, 95–108 (1997).
[23] Z. S. Wang, G. R. Darling, and S. Holloway, J. Chem. Phys. **120**, 2923–2933 (2004).
[24] C. Díaz, R. A. Olsen, D. J. Auerbach, and G. J. Kroes, Phys. Chem. Chem. Phys. **12**, 6499–6519 (2010).
[25] G. J. Kroes, C. Díaz, E. Pijper, R. A. Olsen, and D. J. Auerbach, Proc. Natl. Acad. Sci. U.S.A. **107**, 20881–20886 (2010).
[26] C. T. Rettner, H. A. Michelsen, and D. J. Auerbach, Chem. Phys. **175**, 157–169 (1993).
[27] Y. Y. Chuang, M. L. Radhakrishnan, P. L. Fast, C. J. Cramer, and D. G. Truhlar, J. Phys. Chem. A **103**, 4893–4909 (1999).
[28] J. P. Perdew, J. A. Chevary, S. H. Vosko, K. A. Jackson, M. R. Pederson, D. J. Singh, and C. Fiolhais, Phys. Rev. B **46**, 6671–6687 (1992).
[29] B. Hammer, L. B. Hansen, and J. K. Nørskov, Phys. Rev. B **59**, 7413–7421 (1999).
[30] K. Honkala, A. Hellman, I. N. Remediakis, A. Logadottir, A. Carlsson, S. Dahl, C. H. Cristensen, and J. K. Norskov, Science **307**, 555–558 (2005).
[31] S. Dahl, A. Logadottir, R. C. Egeberg, J. H. Larsen, I. Chorkendorff, E. Törnqvist, and J. K. Nørskov, Phys. Rev. Lett. **83**, 1814–1817 (1999).
[32] G. Jones *et al.*, J. Catal. **259**, 147–160 (2008).
[33] G. Comsa and R. David, Surf. Sci. **117**, 77–84 (1982).
[34] G. Anger, A. Winkler, and K. D. Rendulic, Surf. Sci. **220**, 1–17 (1989).
[35] H. A. Michelsen and D. J. Auerbach, J. Chem. Phys. **94**, 7502–7520 (1991).
[36] L. Schröter, C. Trame, J. Gauer, H. Zacharias, R. David, and W. Brenig, Faraday Discuss. **96**, 55 (1993).
[37] S. Küchenhoff and W. Brenig, Surf. Sci. **258**, 302 (1991).
[38] J. Kim and G. O. Sitz, Mol. Phys. **108**, 1027–1032 (2010).
[39] G. J. Kroes, E. J. Baerends, and R. C. Mowrey, Phys. Rev. Lett. **78**, 3583–3586 (1997).
[40] D. A. McCormack and G. J. Kroes, Phys. Chem. Chem. Phys. **1**, 1359–1374 (1999).
[41] D. A. McCormack, G. J. Kroes, E. J. Baerends, and R. C. Mowrey, Faraday Discuss. **110**, 267–285 (1998).
[42] D. A. McCormack, G. J. Kroes, R. A. Olsen, E. J. Baerends, and R. C. Mowrey, J. Chem. Phys. **110**, 7008–7020 (1999).
[43] D. A. McCormack, G. J. Kroes, R. A. Olsen, E. J. Baerends, and R. C. Mowrey, Phys. Rev. Lett. **82**, 1410–1413 (1999).
[44] E. Watts, G. O. Sitz, D. A. McCormack, G. J. Kroes, R. A. Olsen, J. A. Groeneveld, J. N. P. v. Stralen, E. J. Baerends, and R. C. Mowrey, J. Chem. Phys. **114**, 495–503 (2001).
[45] M. F. Somers, R. A. Olsen, H. F. Busnengo, E. J. Baerends, and G. J. Kroes, J. Chem. Phys. **121**, 11379–11387 (2004).
[46] M. F. Somers, D. A. McCormack, G. J. Kroes, R. A. Olsen, E. J. Baerends, and R. C. Mowrey, J. Chem. Phys. **117**, 6673–6687 (2002).
[47] D. A. McCormack, G. J. Kroes, R. A. Olsen, J. A. Groeneveld, J. N. P. van Stralen, E. J. Baerends, and R. C. Mowrey, Chem. Phys. Lett. **328**, 317–324 (2000).
[48] M. F. Somers, D. Lemoine, and G. J. Kroes, Chem. Phys. **304**, 59–77 (2004).
[49] T. Sahoo, S. Sardar, and S. Adhikari, Phys. Chem. Chem. Phys. **13**, 10100–10110 (2011).
[50] T. Sahoo, S. Sardar, P. Mondal, B. Sarkar, and S. Adhikari, J. Phys. Chem. A **115**, 5256–5273 (2011).
[51] E. Fromm and E. Gebhardt, *Gase und Kohlenstoff in Metallen* (Springer, Heidelberg, 1976).
[52] A. C. Allison and A. Dalgarno, At. Data **1**, 289 (1969).
[53] J. E. Hesser, J. Chem. Phys. **48**, 2518 (1968).
[54] L. Schröter, Chr. Trame, R. David, and H. Zacharias, Surf. Sci. **272**, 229 (1992).
[55] C. H. Greene and R. N. Zare, Annu. Rev. Phys. Chem. **33**, 119 (1982).
[56] See supplementary material at http://dx.doi.org/10.1063/1.4776224 for a detailed discussion of the model and how quantities that are comparable to observables measured in molecular beam experiments and associative desorption can be obtained from computed initial state-resolved reaction probabilities $R_{v\,j\,m_j}(E)$ and degeneracy averaged reaction probabilities $R_{v\,j}(E)$.
[57] G. J. Kroes, G. Wiesenekker, E. J. Baerends, and R. C. Mowrey, Phys. Rev. B **53**, 10397 (1996).
[58] G. R. Darling and S. Holloway, J. Chem. Phys. **97**, 734 (1992).
[59] G. R. Darling and S. Holloway, Surf. Sci. **307**, 153 (1994).
[60] H. F. Berger, Ph.D. dissertation, Technische Universität Gratz, 1992.
[61] K. D. Rendulic and A. Winkler, private communication (2012).
[62] H. F. Berger, M. Leisch, A. Winkler, and K. D. Rendulic, Chem. Phys. Lett. **175**, 425 (1990).
[63] A. Gross, B. Hammer, M. Scheffler, and W. Brenig, Phys. Rev. Lett. **73**, 3121 (1994).

[64]M. Karikorpi, S. Holloway, N. Henriksen, and J. K. Nørskov, Surf. Sci. **179**, L41 (1987).
[65]P. Kratzer, B. Hammer, and J. K. Norskov, Surf. Sci. **359**, 45 (1996).
[66]C. T. Rettner, H. A. Michelsen, and D. J. Auerbach, J. Chem. Phys. **102**, 4625 (1995).
[67]C. Díaz *et al.*, "Comparison of theoretical and experimental desorption energies for H_2 desorbing from Cu(100) and Cu(111)," J. Chem. Phys. (to be published).
[68]H. A. Michelsen, C. T. Rettner, D. J. Auerbach, and R. N. Zare, J. Chem. Phys. **98**, 8294 (1993).
[69]G. R. Darling and S. Holloway, J. Chem. Phys. **101**, 3268 (1994).
[70]H. Hou, S. J. Goulding, C. T. Rettner, A. M. Wodtke, and D. J. Auerbach, Science **277**, 80 (1997).
[71]C. Díaz, R. A. Olsen, H. F. Busnengo, and G. J. Kroes, J. Phys. Chem. C **114**, 11192 (2010).
[72]G. Sitz, private communication (2012).